NeuroImage 254 (2022) 119128

Contents lists available at ScienceDirect

NeuroImage

journal homepage: www.elsevier.com/locate/neuroimage

Network dynamics scale with levels of awareness

Peter Coppola[a,b], Lennart R.B. Spindler[a,b], Andrea I. Luppi[a,b], Ram Adapa[a,c], Lorina Naci[d], Judith Allanson[b,e], Paola Finoia[a,c], Guy B. Williams[b,f], John D. Pickard[b,c,f], Adrian M. Owen[g], David K. Menon[a,f], Emmanuel A. Stamatakis[a,b,*]

[a] Division of Anaesthesia, School of Clinical Medicine, Addenbrooke's Hospital, University of Cambridge, Hills Rd., Cambridge CB2 0QQ, UK
[b] Department of Clinical Neurosciences, School of Clinical Medicine, Addenbrooke's Hospital, University of Cambridge, Hills Rd., Cambridge CB2 0QQ, UK
[c] Division of Neurosurgery, School of Clinical Medicine, Addenbrooke's Hospital, University of Cambridge, Hills Rd., Cambridge CB2 0QQ, UK
[d] Trinity College Institute of Neuroscience, School of Psychology, Trinity College Dublin, Lloyd Building, Dublin 2, Ireland
[e] Department of Neurosciences, Addenbrooke's Hospital, Cambridge University Hospitals NHS Foundation, Hills Rd., Cambridge, CB2 0QQ, UK
[f] Wolfson Brain Imaging Centre, University of Cambridge, Cambridge Biomedical Campus (Box 65), Cambridge CB2 0QQ, UK
[g] The Brain and Mind Institute, Western Interdisciplinary Research Building, University of Western Ontario, London, ON N6A 5B7, Canada

ARTICLE INFO

Keywords:
Consciousness
Network science
Network dynamics
Subcortex
Small world
Participation coefficient
Cerebellum

ABSTRACT

Small world topologies are thought to provide a valuable insight into human brain organisation and consciousness. However, functional magnetic resonance imaging studies in consciousness have not yielded consistent results. Given the importance of dynamics for both consciousness and cognition, here we investigate how the diversity of small world dynamics (quantified by sample entropy; dSW-E[1]) scales with decreasing levels of awareness (i.e., sedation and disorders of consciousness). Paying particular attention to result reproducibility, we show that dSW-E is a consistent predictor of levels of awareness even when controlling for the underlying functional connectivity dynamics. We find that dSW-E of subcortical, and cortical areas are predictive, with the former showing higher and more robust effect sizes across analyses. We find that the network dynamics of intermodular communication in the cerebellum also have unique predictive power for levels of awareness. Consequently, we propose that the dynamic reorganisation of the functional information architecture, in particular of the subcortex, is a characteristic that emerges with awareness and has explanatory power beyond that of the complexity of dynamic functional connectivity.

1. Introduction

Recent neuroscience endeavours have approached the intractable question of consciousness via notions of complexity (Carhart-Harris et al., 2014; Northoff and Huang, 2017; Tononi et al., 2016; Varley et al., 2020). A complex system can be defined as a large network of components that exhibit collective emergent properties (Mitchell, 2011). In fact, consciousness researchers have focused their attention not only on the activity of brain regions; but also the statistical relationship between them (i.e., "connectivity") and the resulting emergent global properties (Tononi et al., 2016; Edelman and Gally, 2013; Di Perri et al., 2016; Stamatakis et al., 2010).

A prominent paradigm to investigate the complexity of brain connectivity is given by network science (Rubinov and Sporns, 2010; Watts and Strogatz, 1998). Using the mathematical framework of Graph Theory Analysis (GTA), network science permits an investigation into the topological/architectural characteristics of a network by defining its components as nodes and their interactions as edges. Watts and Strogatz (1998) brought this approach to the forefront by showing that complex real-life networks of the most disparate kinds tend to show a "small-world" (SW) architecture. Computationally, the SW network structure can be created by taking a regular lattice network (where neighbouring nodes are connected) and randomly rewiring some edges. This particular network configuration simultaneously retains many clusters of connected nodes, whilst the rewired edges enable information to travel easily across long distances in the network (i.e., an average "short path length"). The SW network is appealing to neuroscience as it putatively describes the fundamental local-global interaction of a limited number of brain regions and connections, and thus would allow complexity to emerge in a cost-effective manner (Northoff and Huang, 2017; Sporns and Zwi, 2004; van den Heuvel et al., 2008; Bassett and Bullmore, 2017). In fact, SW topology has been shown to favour synchronisation, richness of possible states, self-organisation,

* Corresponding author at: Division of Anaesthesia, School of Clinical Medicine, Addenbrooke's Hospital, University of Cambridge, Hills Rd., Cambridge CB2 0SP, UK.
E-mail address: eas46@cam.ac.uk (E.A. Stamatakis).

[1] dSW-E= dynamic small world entropy

https://doi.org/10.1016/j.neuroimage.2022.119128.
Available online 22 March 2022.

criticality, resistance to insult, efficient and cost-effective information transfer (Papo et al., 2016; Tan and Cheong, 2017; Barahona et al., 2002; Takagi, 2018; Takagi, 2020).

Given these characteristics, theorists have conjectured that SW organisation is relevant to consciousness (Northoff and Huang, 2017; Sporns and Zwi, 2004; Carhart-Harris and Friston, 2019; Buzsáki, 2007; Alkire et al., 2008). In fact, SW is a topology (i.e., interrelation of constituent parts) that indicates simultaneous localised-clustered (segregated) and efficient-global (integrated) information flow (Northoff and Huang, 2017; Rubinov and Sporns, 2010; Bassett and Bullmore, 2017; Lord et al., 2017; Deco et al., 2015). Theoretically, dynamic integration would underpin the sense of unified experience, whilst segregation of specialised information would underlie the vast variety of perceptual and phenomenal distinctions that can be experienced (Northoff and Huang, 2017; Tononi et al., 2016; Sporns and Zwi, 2004; Dehaene and Christen, 2011; Baars, 2005). Therefore, SW has been thought to underlie the spatial temporal characteristics necessary for the emergence of awareness (Northoff and Huang, 2017; Buzsáki, 2007; Alkire et al., 2008).

The empirical side, conversely, has proposed several measures of SW architecture (Humphries and Gurney, 2008; Muldoon et al., 2016; Telesford et al., 2011); but has not yielded the same level of consistency as its theoretical counterpart. Research in the functional network SW of anaesthesia has shown increases in SW during unconsciousness, in opposition to what would have been expected from theory (Northoff and Huang, 2017; Schroter et al., 2012; Monti et al., 2013). Others show decreases in SW during anaesthesia and disorders of consciousness (Luppi et al., 2019; Barttfeld et al., 2015). Still more papers report inconclusive SW results in consciousness-relevant conditions (Achard et al., 2012; Crone et al., 2014; Godwin and Barry, 2015). There are also contradicting results arising from structural connectivity measurements of SW configurations (Weng et al., 2017; Tan et al., 2019).

The brain is characterised by constantly changing dynamical interactions (Supplementary movie; James (1890)). Analogously to the proposed importance of SW topology to dynamic information flow (Watts and Strogatz, 1998; Bassett and Bullmore, 2017; Tan and Cheong, 2017; Barahona et al., 2002; Takagi, 2018), different theories of consciousness converge in proposing that the dynamic richness of possible brain states is a fundamental hallmark of consciousness (Carhart-Harris et al., 2014; Northoff and Huang, 2017; Tononi et al., 2016; Dehaene and Christen, 2011). The study of dynamics in consciousness research has in fact proven empirically successful (Luppi et al., 2019; Barttfeld et al., 2015; Huang et al., 2020; Demertzi et al., 2019; Golkowski et al., 2019; Cavanna et al., 2018; Crone et al., 2020) and there is some evidence of how disruption of small-world topology may occur in consciousness in particularly integrated states (Luppi et al., 2019). Furthermore, there is evidence that the temporal variability of the clustered-segregated component of SW topology is reduced in unconsciousness due to brain injury (Crone et al., 2020).

Although SW structure is universally recognised as important for network dynamics (Watts and Strogatz, 1998; Tan and Cheong, 2017; Barahona et al., 2002; Takagi, 2018), most studies of consciousness looking into such network topologies have primarily focused on static networks (Schroter et al., 2012; Monti et al., 2013; Achard et al., 2012; Crone et al., 2014), networks clustered across time (Luppi et al., 2019) or have not assessed unique predictive power of different measures in different subsystems and states of consciousness (Crone et al., 2020).

To tackle the inconsistencies between different empirical studies and theory, and to probe the relevance of network science to consciousness, we investigated the dynamics of small-worldness (SW). Given the dynamic nature of subjective phenomenology and the brain, and the balance between integration and segregation being proposed as essential to unified experience (Tononi and Edelman, 1998), we hypothesised that the temporal complexity of small worldness would be a strong predictor of levels of awareness. Such network dynamics may relate to a fundamental mechanism (integration and segregation) in producing the (dynamically varying) stream of consciousness. Thus, we reduce the high dimensionality of connectivity data to properties that describe network architecture in terms of integration and segregation. To investigate how complex ("unpredictable" or "uncompressible") network architectures are over time, we use an information-theory measure adapted to biological dynamical systems, namely sample entropy (Delgado-Bonal and Marshak, 2019; Richman and Moorman, 2000). This metric, previously employed for fMRI data (e.g., Richman and Moorman, 2000; Omidvarnia et al., 2021; Wang et al., 2014; Pedersen et al., 2017), has been shown to be robust in noisy and short timeseries and specifically considers temporal contiguous information (unlike previously employed approaches, Crone et al., 2020). Sample entropy has also been shown to be correlated to other measures of complexity indicating that it is robust and may successfully be used to measure underlying complexity ((Varley et al., 2020); see section 2.6 for more details).

Given previous inconsistencies in this area, we devote particular attention to convergence of SW results by deploying different brain parcellations (i.e., region definitions that form network nodes), measures and datasets. Parcellations, which varied between the aforementioned SW studies (Schroter et al., 2012; Monti et al., 2013; Luppi et al., 2019), have been known to affect graph theory results (Papo et al., 2016; Yao et al., 2015; Hallquist and Hillary, 2018; Luppi and Stamatakis, 2020). Therefore, the employment of different parcellations to assess whether results are parcellation-dependent is advised (Hallquist and Hillary, 2018). We used whole-brain parcellations with different granularities (i.e., Low and high granularity, 126 and 553 brain regions, respectively, described in Appendix A, and, respectively, named WB126 and WB553) and the AAL (Automatic Anatomical Labelling atlas), which has been extensively used in previous literature (Schroter et al., 2012; Luppi et al., 2019; Weng et al., 2017; Tan et al., 2019). To further assess convergence of results we chose to employ two different SW measures: Sigma (σ), as it is the most widely reported measure in the literature (Schroter et al., 2012; Monti et al., 2013; Luppi et al., 2019), and the more recently developed PHI (φ), which displays higher reliability in simulated networks and is designed for biologically-relevant weighted connectivity (Muldoon et al., 2016). Please note this is not "PHI" as defined in the context of integrated information theory (Tononi et al., 2016).

The empirical data consists of three independent functional magnetic resonance imaging (fMRI) datasets that are relevant to consciousness. Two are propofol anaesthesia datasets; the first collected in Cambridge (referred to as "CAM" dataset onwards), UK (18 participants) comprising a control awake and a moderate sedation condition (Adapa et al., 2014) and the second in London, Ontario (henceforth referred to as LON) with 16 participants in control awake and deep sedation conditions (Naci et al., 2018). The third dataset was acquired from patients with disorders of consciousness (hereafter indicated by "DOC", Cambridge, UK). This comprised 23 patients of whom 11 are in a Minimally Conscious State (MCS), and the other 12 diagnosed as Unresponsive Wakefulness Syndrome (UWS).

The use of these different datasets permits us to assess the importance of network dynamics in consciousness independently of the type of consciousness alteration (i.e., pharmacologically or pathologically induced). To this end, these conditions will be ordered according to decreasing levels of awareness (i.e., "content consciousness" Laureys et al., 2007). We predict that the temporal complexity of SW, if relevant to consciousness, will consistently diminish with decreasing levels of awareness, in accordance to theoretical models (Carhart-Harris et al., 2014; Tononi et al., 2016; Laureys et al., 2007). Besides analyses at the whole-brain level, we will also investigate whether these effects are differentially driven by different subsystems (cortex, subcortex, cerebellum), or the connectivity between them. We will also test whether any subsystem effects are exclusive to SW or can be extended to other graph theory measures (namely modularity and participation coefficient) that, similarly to SW, quantify theoretically-relevant functional segregation (functional division/specialisation) and integration (func-

tional combination/information merging) from a network science perspective (Rubinov and Sporns, 2010; Sporns and Zwi, 2004; Luppi et al., 2019; Achard et al., 2012).

2. Methods

2.1. Cambridge anaesthesia dataset (CAM)

2.1.1. Participants – CAM dataset

Ethical approval was obtained from the Cambridgeshire 2 Regional Ethics committee (Adapa et al., 2014). 25 participants were recruited, however due to incomplete data in the cortex and procedure failure, a subset of 18 were taken for further analyses. All participants were healthy and were native English speakers (50% males). Mean age was 33.3. ; ; ; Two senior anaesthetists were present during scanning. Electrocardiography and pulse oximetry were continuously performed whilst measures of blood pressure, heart rate and oxygen saturation were recorded regularly.

2.1.2. Anaesthetic protocol – CAM dataset

Propofol sedation was administered intravenously via "target controlled infusion" with a Plasma Concentration mode. An Alaris PK infusion pump (Carefusion, Basingstoke, UK) was used which was controlled via the Marsh pharmacokinetic model. The anaesthesiologist can thus decide on a desired plasma 2 "target" and the system will regulate the infusion rates using patient characteristics as covariates. Three target plasma levels were used – no drug (awake control), 0.6 μg/ml (low sedation), 1.2 μg/ml (moderate sedation). In this study only the moderate sedation condition is used. Data for this latter condition was taken 20 min after cessation of sedation. Blood samples were taken at the end of each titration period, before plasma target was altered. The level of sedation was probed verbally immediately before and after each of the scanning runs.

10 min of plasma and effect-site propofol concentration equilibration was allowed before cognitive tests were commenced (auditory and semantic decision tasks). Mean (standard deviation) plasma propofol concentrations was 304.8 (141.1) mg/ml during light sedation, 723.3 (320.5) mg/ml during moderate sedation and 275.8 (75.42) mg/ml during recovery. Mean (SD) total propofol given was 210.15 (33.16) mg.

2.1.3. Magnetic resonance imaging protocol – CAM dataset

A Trio Tim 3 tesla MRI machine (Erlangen, Germany), with 12-channel head coil was used to obtain 32 descending interleaved oblique axial slices with an interslice gap of 0.75 mmm and an in-plane resolution of 3 mm. The field of view was 192 × 192, repetition time and acquisition time was 2 s whilst the echo time (TE) was 30 ms and flip angle 78 degrees. T1-weighted structural images with 1 mm resolution were obtained using an MPRAGE sequence with TR = 2250 ms, TI = 900 ms, TE = 2.99 ms and flip angle = 9°. 150 timepoints were collected for this dataset (an acquisition that lasted 5 min).

2.2. London Ontario propofol (LON) dataset

2.2.1. Participants - LON dataset

The second anaesthesia dataset used was obtained at the Robarts Research Institute in London, Ontario (Canada) and was approved by the Western University Ethics board. 19 healthy (13 males; 18–40 years), right-handed, English speakers with no reported neurological conditions signed an informed-consent sheet and received pecuniary compensation for their time. The study was approved by research ethics boards of Western University (Ontario, Canada). Due to equipment malfunction or impairments with the anaesthetic procedure three participants were excluded (1 male). Thus, 16 participants were included in this study (Naci et al., 2018).

2.2.2. Anaesthetic procedure - LON dataset

The procedure was supervised by two anaesthesiologists and one anaesthetic nurse in the scanning room. Participants also performed an auditory target-detection task and a memory verbal recall to assess level of awareness independently from the anaesthesiologists. Additionally, an infrared camera was used to further assess level of wakefulness.

Propofol was administered intravenously using a Baxter AS50 (Singapore); stepwise increments were applied via a computer-controlled infusion pump until all three assessors agreed that Ramsay level 5 was reached (i.e. no responsiveness to visual or verbal incitements). If necessary, further manual adjustments were made to reach target concentrations of propofol which were predicted and maintained stable by a pharmacokinetic simulation software (TIVA trainer). This software also measured blood concentration levels following the Marsh 3-compartment model. The initial propofol concentration target was 0.6 μg/ml, and step-wise increments of 0.3 μg/ml were applied after which Ramsay score was assessed. This procedure was repeated until participants stopped answering to verbally and where rousable only by physical stimulation at which point data collection would begin. Oxygen titration was put in place to ensure SpO2 above 96%. The mean estimated effect site propofol concentration was 2.48 (1.82–3.14) μg/ml and propofol concentration whilst the mean plasma concentration was 2.68 (1.92–3.44). Mean total mass of propofol administered was 486.58 (1.92–3.44). 8 min of RS-fMRI data was acquired.

2.2.3. Magnetic resonance imaging protocol – LON dataset

A 3-tesla Siemens Trio scanner was used to acquire 256 functional volumes (Echo-planar images [EPI]). Scanning parameters were: slices = 33, 25% inter-slice gap resolution 3 mm isotropic; TR = 2000 ms; TE = 30 ms; flip-angle = 75°; matrix = 64 × 64. Order-of-acquisition was bottom-up interleaved. The anatomical high-resolution T1 weighted images (32-channel coil, 1 mm isotropic voxels) were acquired using a 3D MPRAGE sequence with TA = 5 mins, TE = 4.25 ms, matrix = 240 × 256, 9° FA. This dataset had broadly insufficient cerebellar cover in MRI images. Hence analyses specifically involving the cerebellum were not run for this dataset.

2.3. Disorders of consciousness dataset (DOC)

2.3.1. Patients - DOC dataset

MRI data for 23 DOC patients were collected between January 2010 and July 2015 in the Wolfson Brain Imaging Centre in Addenbrookes Cambridge, UK (mean time post injury 15.75 For UWS and 16.9 for MCS). These were selected out of a bigger dataset ($n = 71$) due to their relatively intact neuroanatomy. These patients were treated and scanned at the Wolfson Brain Imaging Centre, Addenbrookes Hospital (Cambridge, UK). Written informed consent was obtained from an individual that had legal responsibility on making decisions on the patient's behalf. These participants were split into unresponsive wakefulness syndrome and minimally conscious state groups ($n = 12$ for UWS and $n = 11$ for MCS) in accordance to the diagnosis given by the attending physician at Addenbrookes Hospital. Mean CRS-r score was 8.3 (standard deviation 2.03). For the UWS group CRS-r score was 7, (1.41) and 9.75 (1.54) for the MCS group. Mean age for the UWS group was 40.16 (13.63); and for the MCS group 39.18 (18.13). In the UWS group the aetiology was described as TBI for 3 patients, one hypoxia, one oedema and the remaining participants having the pathology caused by anoxia. In the MCS group nine of the patients had a traumatic brain injury, one a cerebral bleed and one anoxia. In the MCS group 7 were male; whilst in the UWS group 8 were male. This dataset received ethical approval from the National Research Ethics Service.

2.3.2. Magnetic resonance imaging protocol - DOC dataset

A varying number of functional tasks, anatomical and diffusion MRI images were taken for the DOC participants. Only the resting-state data was used for this study. This was acquired for 10 min (300 vol, TR = 2 s)

using a siemens TRIO 3T scanner. The functional images were acquired using an echo planar sequence. Parameters include: 3 × 3 × 3.75 mmm resolution, TR/TE = 2000 ms/30 ms, 78° FA. Anatomical images T1-weighted images were acquired using a repetition time of 2300 ms, TE = 2.47 ms, 150 slices with a cubic resolution of 1 mm.

2.4. Preprocessing

All functional images were preprocessed in the same way using an in-house Matlab script that used SPM12 functions (https://www.fil.ion.ucl.ac.uk/spm/software/spm12). After removing the first 5 scans to reach scanner equilibrium, slice-timing correction was performed (reference slice = no. 17, chosen as it corresponded to the middle [axially] of the brain). Volumes were realigned to the mean functional image. This process produced re-alignment parameters which were included in the time series extraction covariates (described in Section 2.4.1). Finally, using the mean functional image, spatial normalization to an EPI-template was conducted using the function "old norm" in SPM as this yielded consistently good results in comparison to other approaches when assessed visually (similarly to a previous study Calhoun et al., 2017). Participant-specific cerebral spinal fluid and white matter maps, used for the time series extraction (See Section 2.4.1), were also created using an in-house Matlab (2016a) script based on SPM functions. Visual inspection of normalization to standard space was carried for all datasets. Particular attention was given to the DOC dataset because of the effect that lesions may have on spatial transformations. Due to insufficient coverage of the cerebellum in one UWS patient, they were excluded from analyses involving the cerebellum to avoid bias in results.

2.4.1. Time series extraction

Denoising steps were performed in the Matlab and SPM-based software CONN (17.f) (https://web.conn-toolbox.org/). It is very important to remove motion-induced artefacts in fMRI data, especially in DOC data which may display inordinate amount of movement (Weiler et al., 2021). We applied several methods to ensure movement did not unduly influence the independent variables. Firstly, movement parameters and their first temporal derivative were included as a first-level covariate so as to remove movement-related noise. The aCompCorr algorithm regressed out CSF, white-matter and motion-related signals from the time-series (using the first 5 principal components; default setting in CONN). This method been shown to perform well in removing movement, respiratory and cardiac artifacts (Power et al., 2018), especially on DOC patients (Weiler et al., 2021) and has been previously used for this type of data (Luppi et al., 2019; Crone et al., 2020). The ART quality-assurance/motion-artefact rejection toolbox (https://www.nitrc.org/projects/artefact_detect), as implemented in CONN, was also used to further remove motion-related artifacts in the timeseries data. This method involves regressing out the effect of outlier scans (movement > 0.09 mm) in a first-level analysis which is suggested to further reduce focal effects of movement that are not accounted for by the aCompCorr algorithm (Power et al., 2018; Parkes et al., 2018).

Linear de-trending and a commonly used 0.008–0.09 Hz band-pass filter was applied (default in CONN and a widely adopted choice in the literature on resting-state fMRI) to eliminate low-frequency scanner drifts and potential high-frequency noise. The time-series were extracted controlling for the nuisance variables described above from the unsmoothed functional volumes to avoid artificially-induced correlations in clustered regions of interests.

2.5. . Graph theory analysis: graph construction

Graph theory analyses were run on weighted thresholded undirected connectivity matrices (i.e., graphs). The regions of interest (ROI) corresponded to "nodes" and are placed on the rows and columns of a matrix; whilst the Pearson's correlations (as is typically used in the literature) between any two pairs of nodes were considered weighted (functional connectivity; FC) edges and are represented by the cells in the matrix (Rubinov and Sporns, 2010; Luppi and Stamatakis, 2020). Self-connections were set to 0 and NaN values were removed to ensure graphs represented ROI-to-ROI connections.

There is no consensus regarding how to threshold connectivity matrices (Rubinov and Sporns, 2010; Monti et al., 2013; Crone et al., 2014). Usually a set of thresholds are used to ensure that results are consistent and not driven by graph topologies at specific connection densities (Rubinov and Sporns, 2010; Hallquist and Hillary, 2018; van den Heuvel et al., 2017). Proportional thresholding was used (e.g., top 10% of correlations). This ensures that the networks compared are of the same size, have similar properties such as node-connectivity distribution, and that the density of each network was calculated relative to its size (Rubinov and Sporns, 2010; Hallquist and Hillary, 2018). There have been critiques (Hallquist and Hillary, 2018; van den Heuvel et al., 2017) to the use of proportional thresholding in clinical populations as baseline functional connectivity may be different compared to controls and would introduce spurious effects in the network analysis. It is possible, that graph theory differences are actually driven by simple FC differences. To obviate this problem, other than controlling for dynamic FC entropy at the inferential statistic level, weighted networks were used as lower correlations would have lower influence on the calculation of GTA metrics and are reported to ameliorate FC-driven GTA differences (van den Heuvel et al., 2017).

To further guard from the problem of the FC-driven GTA differences, a particularly stringent proportional threshold was used to define graphs. 5 thresholds going from 5% to 25% in 5% incremental steps were used to test a wide-range of connection densities and ensure results are not driven by any particular arbitrarily-chosen threshold (Rubinov and Sporns, 2010; Monti et al., 2013; Godwin and Barry, 2015; Luppi and Stamatakis, 2020). Given the lack of knowledge as to the most appropriate range of thresholds for graph theory analyses, we took this range from previous studies (Monti et al., 2013; Godwin and Barry, 2015). Of note is that a previous study investigating the sample entropy of graph theory dynamics showed results to be stable across similarly defined thresholds (Pedersen et al., 2017). Additionally, we calculated threshold specific results for dynamic small world complexity and its underlying measures (clustering coefficient and path length) and similarly found the results to be stable across these thresholds (appendix B).

This procedure led to 5 functional connectivity matrices for each subject in each timepoint. On each of these connectivity matrices graph theory metrics were calculated, thus reducing the multidimensional graph into a single value describing its topology. Sample entropy (described below, Section 2.6) was calculated on the timeseries of each of these threshold-specific graph theory measures and then averaged to form the independent variables in inferential analyses. The averaging across threshold-specific sample entropy values will reduce the influence of any single threshold on the results. Only positive correlations were considered as is typical for network neuroscience due to the dubious interpretation and the preprocessing contingencies associated with negative weights (Rubinov and Sporns, 2010; Huang et al., 2020; Dixon et al., 2017).

These weighted-thresholded matrices were analysed using in-house matlab scripts which utilised functions from the brain connectivity toolbox (Rubinov and Sporns, 2010). In accordance to previous advice (Hallquist and Hillary, 2018), given how GTA results may be driven by specific parcellations (Papo et al., 2016; Yao et al., 2015; Hallquist and Hillary, 2018), the reproducibility of GTA results was tested through the use of several network definitions (namely WB126, WB553 and the AAL, see appendix A). In evaluating the generalisability of cortical parcellations, a study from our group showed a parcellation with about 200 regions may be the most representative (Luppi and Stamatakis, 2020). Here we followed a different strategy, showing that our results are robust even to substantial changes in parcellation scale

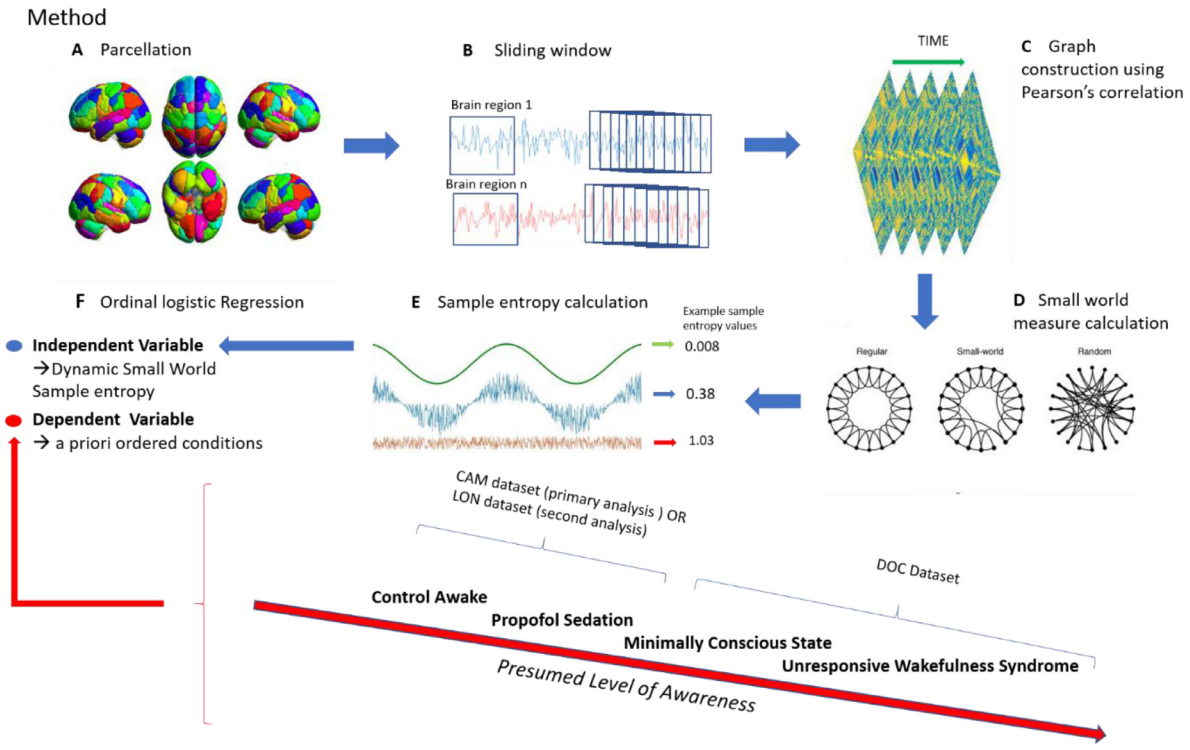

Fig. 1. Illustration of method. A) We obtained timeseries for each brain region. B) The timeseries were divided with a sliding window approach (each window comprising of 24 timepoints and slid by 1 timepoint). C) We then correlated all region timeseries to obtain a weighted graph for each window. D) We calculated SW (Humphries and Gurney, 2008a; Muldoon et al., 2016; Watts and Strogatz, 1998) for each graph so as to obtain a timeseries of SW values on which E) we calculated sample entropy. F) We inserted the sample entropy of dynamic small worldness into an ordinal logistic regression as a predictor; with the ordered conditions (according to presumed level of awareness) as a dependant variable.

(100 and 400). In fact, these parcellations were chosen due to their difference in granularity.

To evaluate the network properties of between subsystem graphs (i.e., cortex-cerebellum, cortex-subcortex and subcortex-cerebellum, results in Section 3.5) we set to zero the irrelevant functional connectivity values in the graph. This procedure was necessary given that uniquely extracting the between network connectivity would have led to non-symmetrical graphs which is not feasible for graph theory analyses. To threshold the graphs, we ordered the functional connectivity values and found the value corresponding to the relevant percentile (used in proportional thresholding; e.g., 5%) of non-zero values. We then inserted this value into the absolute_thresholding.m function of the brain connectivity toolbox (Rubinov and Sporns, 2010). This ensured that the values which were not relevant to the specific between subsystem graph did not influence the procedure of obtaining sparse networks. We did not run the between subsystem analyses on the LON dataset due to insufficient coverage of the cerebellum.

For the creation of time-varying (dynamic) connectivity matrices, a sliding-window approach was used. In accordance with previous studies (Luppi et al., 2019; Preti et al., 2017), the timeseries were split into a window composed of 24 timepoints (48 s) (Fig. 1) which was then moved by one timepoint. Previous studies have suggested that sliding windows between 30 and 60 s capture dynamic functional connectivity fluctuations in a robust manner (Preti et al., 2017). The window sliding (i.e., step) of one timepoint was chosen as it maximised the length of the timeseries of graph theory properties. The timeseries were tempered with a Gaussian window to ensure that the timepoints at the edge of the windows did not have a great effect on the correlations obtained following suggestions from previous studies (Preti et al., 2017).

This procedure resulted in 122 graphs for each participant in the CAM dataset, 271 graphs for the DOC dataset and 251 for the LON dataset. The measure used (sample entropy) upon the properties of these graphs (See Section 2.6; Richman and Moorman, 2000) is stable across differing numbers of time points.

For the sample entropy of functional connectivity (dFC-E), the mean of the positive values for each unthresholded temporally-specific FC matrix was calculated giving a timeseries of FC values on which sample entropy was calculated. Positive values were chosen for the calculation of dFC-E because the graph theory metrics employed in this study used positive edges exclusively (Rubinov and Sporns, 2011) and because proportional thresholding, despite retaining the same number of edges, may retain significantly different positive average connectivity values across clinical conditions and individuals, which may in turn influence graph theory results (Hallquist and Hillary, 2018; van den Heuvel et al., 2017).

2.5.1. Graph theory properties: definitions

Small-worldness attempts to quantify a particular topology of self-organising complex systems (Watts and Strogatz, 1998). This particular architecture is defined by a high clustering-coefficient and a small characteristic path length.

Clustering-coefficient is defined as the fraction of neighbours of a node that are also neighbours (Rubinov and Sporns, 2010; Watts and Strogatz, 1998; Humphries and Gurney, 2008; Muldoon et al., 2016; Telesford et al., 2011) effectively operationalized as:

$$Ci = \frac{2ti}{ki(ki-1)} \quad (1)$$

Where *t*, the number of connected triangles of node *i*, is compared to the number of connections (k) of that node. The clustering coefficient is averaged across nodes to the typical "cliquishness" of a network (Watts and Strogatz, 1998; Humphries and Gurney, 2008; Muldoon et al., 2016; Telesford et al., 2011). The function clustering_coef_wu.m from the brain connectivity toolbox (Rubinov and

Sporns, 2010) was used to calculate this. This clustering algorithm cannot be used in between subsystem graphs (e.g., cortex-subcortex) as there is an impossibility to form triangles when between system edges are considered exclusively (e.g., cortical node A is connected to subcortical node A; cortical node A is connected to subcortical node B; subcortical node B and A cannot be connected as there are no within subsystem edges).

Characteristic path-length is calculated as the average of the shortest distance between all pairs of nodes (Watts and Strogatz, 1998) using Dijkstra's algorithm and is denoted as L. Small values of L indicate that information is readily available (easily transmissible) across the network (Rubinov and Sporns, 2010; Telesford et al., 2011). The charpath function from the brain connectivity toolbox was used to calculate this.

It is common practice to normalise L and C to equivalent (i.e. with comparable network properties) Erdos-Renyi random networks (*Crand* & *Lrand;* Humphries and Gurney, 2008; Schroter et al., 2012; Monti et al., 2013). This ensures that the clustering coefficient and path-length rather than other network properties influence SW, and thus somewhat operationalises the original SW definition (i.e., C >> Crand & $L \geq$ Lrand Watts and Strogatz, 1998; Humphries and Gurney, 2008). The randomisation parameters and the number of random networks created were assessed in terms of convergence of values (i.e., recalculating with increasing values until results were consistently similar). Each Crand and Lrand were calculated from 50 random networks from a rewiring parameter of 5 (in the ranmio_und.m function in brain connectivity toolbox).

The ratio between these random-network normalized values of these gives small-worldness:

$$\sigma = \frac{\gamma}{\lambda} = \frac{\frac{C}{Crand}}{\frac{L}{Lrand}} \tag{2}$$

Thus, the shorter the normalised path-length (λ) and the higher the normalised clustering coefficient (γ), the higher SW-σ. Sigma could not be run on the higher granularity parcellation due to extreme computational requirements.

However, despite being extensively used in the literature (Lord et al., 2017; Schroter et al., 2012; Monti et al., 2013; Luppi et al., 2019), this metric has been criticized as σ is highly dependant on small variations of clustering-coefficient in the random network and is a measure that is primarily driven by clustering coefficient (Papo et al., 2016; Telesford et al., 2011). It is argued that Crand is an inappropriate normalisation model as high clustering is found in lattice networks and in fact in the original definition compares the clustering coefficient of a SW network to that of a lattice network and the path length to a random graph (Watts and Strogatz, 1998). Therefore, Telesford et al. (2011) suggest normalising C to the clustering coefficient of an equivalent lattice network (Clatt).

In fact, for this study the alternative function to calculate small world topology was taken from Muldoon and colleagues (Muldoon et al., 2016), which similarly to Telesford and colleague's measure (Telesford et al., 2011), uses both lattice and random networks to normalise C and L. However, they employ a more complete normalisation method which is more faithful to the original definition of SW (Watts and Strogatz, 1998) than sigma and more suitable for the analysis of weighted connectivity matrices (See appendix C and Section 3.3 for more information).

$$\begin{aligned} \Delta C &= \frac{Clatt-Cobs}{Clatt-Crand} \\ \Delta L &= \frac{Cobs-Lrand}{Llatt-Lrand} \end{aligned} \tag{3}$$

Where L and C indicate path length and clustering coefficient, respectively, of the observed network (obs), an equivalent lattice network (latt), and a random network (rand). These normalisations in turn give the SW measure which ranges from 0 to 1 (the algorithm forces values to 1 in the cases they are above this value):

$$\phi = 1 - \sqrt{\frac{\Delta C^2 + \Delta L^2}{2}} \tag{4}$$

For further conceptual and statistical evaluation of the two small-world measures used in this study see appendix C.

The modularity algorithm (Rubinov and Sporns, 2010; function modularity_und.m, from the brain connectivity toolbox) works by detecting the (computationally) optimal community structure by dividing the network into groups of nodes with maximised within-group connections and minimised between-group connection. Here we used the weighted version of modularity to conserve relevant FC strength information (Rubinov and Sporns, 2010).

$$Q^w = \frac{1}{lw} \sum_{i,j \in N} \left[W_{ij} - \frac{K_j^w K_i^w}{l^w} \right] \delta_{m_i,m_j} \tag{5}$$

Where l is the number of links, i and j represent nodes, W the weights, and K the degree and the δ_{m_i,m_j} parameter is 1 if the nodes i and j are in the same module and 0 otherwise.

The participation coefficient is a measure of the richness of intermodular connectivity of all nodes, and requires modularity to have been calculated already (Rubinov and Sporns, 2010). The participation_coef.m function was used in this study (Rubinov and Sporns, 2010).

$$y_i^w = 1 - \sum_{m \in M} \left(\frac{k_i^w(m)}{k_i^w} \right)^2 \tag{6}$$

Where M is the set of modules, k_i^w (m) is number of weighted links between i and all nodes in module m.

All metrics were calculated across the 5 thresholded networks for each timepoint. All graph theory measures, excepting the SW propensity (Muldoon et al., 2016), were calculated using the brain connectivity toolbox (Rubinov and Sporns, 2010).

2.6. Sample entropy

In dynamical systems, entropy is a measure of the rate of information produced. Sample entropy was developed specifically to obviate the problem of having short and noisy timeseries which is typical of biological datasets (Delgado-Bonal and Marshak, 2019; Richman and Moorman, 2000), and therefore makes it particularly suitable to fMRI derived timeseries analysis (Luppi et al., 2019; Wang et al., 2014). It additionally considers sequential information in the timeseries rather than the distribution (e.g., Shannon entropy or standard deviation Waschke et al., 2021) making it appropriate for analysis of the complexity of a dynamical system (Richman and Moorman, 2000). This measure has been shown to relate to other measures of complexity (Varley et al., 2020) indicating it is adept to detecting underling complexity. Furthermore, it has been shown to correlate with fluid intelligence and in-scanner behaviour, to be reproducible across different fMRI sessions and to maintain robustness across different parameters (Omidvarnia et al., 2021; Wang et al., 2014; Pedersen et al., 2017; Zhang et al., 2020). For these reasons we have selected it as the complexity measure of network property timeseries. Sample entropy is an improvement on approximate entropy, which in turn is based upon Kolomogorov complexity (Mitchell, 2011; Kolmogorov, 1965). The underlying notion being that a complex system cannot be easily described, whilst a simple system can be quickly or briefly summarized.

Sample entropy takes two timeseries segments of different lengths and compares how well each of these segments explains the rest of the timeseries (via the Chebyshev distance measure, chosen as it was the default in the code obtained from the original creators Richman and Moorman (2000)). Sample entropy is a ratio between how well the smaller segment explains the data compared to the larger segment, and thus higher values indicating decreased self-similarity and increased complexity.

$$SampEn = -log \frac{A}{B} \tag{7}$$

Where A is how similar the smaller timeseries segment (via Chebyshev distance) to the rest the timeseries. B is how similar the bigger timeseries segment relates to the rest of the timeseries.

The sequence lengths or timeseries lengths (max = 2, min = 1) were taken from a study which has looked at sample entropy of graph theory properties in functional MRI (Pedersen et al., 2017). Whilst the authors report that these parameters can produce replicable results across independent datasets, there is still no consensus as to how to select optimal parameters. Also taken from this study is the tolerance for accepting matches of similarity which was set to 0.2 times the standard deviation. This permits the comparison of signals with different amplitudes (Richman and Moorman (2000), appendix C) and such a scaling of this threshold by the standard deviation of the signal is also used by the original creators of the sample entropy algorithm (Richman and Moorman, 2000). The algorithm used in this study was used in a previous study with the original creators of the sample entropy algorithm (Lake et al., 2002).

2.7. Inferential analyses: ordinal logistic regression

To assess the hypothesis that the dynamical complexity of graph theory properties diminished with decreasing levels of awareness ordinal logistic regressions were performed using the polr function of the MASS R toolbox. This is a regression model for ordinal categorical dependant variables whilst the independent variable is continuous. This is derived from the logistic regression and is ideally suited to this study given the hypothesis (monotonic decrease of complexity across levels of awareness) and the little assumptions underlying it. Nonetheless, multicollinearity was assessed when multiple predictor variables were included and the proportional odds assumption was tested using Brants test (using package 'brant'). The proportional odds assumption entails the model coefficients have a proportional effect on each group; I.e., "the slope" estimated between each condition (outcome variable) is the same or proportional. All tests were one-sided given the direction-specific hypotheses. To estimate interpretable odds ratio effects sizes, we ordered the conditions from lowest level of awareness to the highest (UWS>MCS>SED>CON). The reason for this was it produced much more interpretable odds ratios (i.e., greater than 1 rather than tending to 0). Odds ratios can be obtained from the regression coefficient independent of ordering via exp(abs(X)), applicable in matlab, r, excel, python etc.

3. Results

In order to confirm that the dynamics of network SW architecture can predict altered levels of awareness, we divided whole brain resting-state fMRI data spatially into different parcellations (Fig. 1A) and then split the resulting timeseries using a sliding window approach (Luppi et al., 2019; Barttfeld et al., 2015; Preti et al., 2017) (Fig. 1B). Within each of these windows we constructed a network by relating each brain region's timeseries to all others, using Pearson's correlation coefficients (Fig. 1C). Two small world measures (*PHI* (Muldoon et al., 2016); and *Sigma* (Humphries and Gurney, 2008), Fig. 1D) were calculated on each of these networks to initially assess the reliability of this approach. In this manner, we obtained a time-series of SW values on which sample entropy was calculated (Richman and Moorman, 2000) (Fig. 1E), thus obtaining one value for each subject that denotes the richness, or complexity, of their SW fluctuations. Inferential statistics were performed using ordinal logistic regressions, with sample entropy values as the predictor variable and ordered conditions as the predicted variable (Fig. 1F).

To assess whether dynamic SW complexity scales with consciousness, we ordered the conditions *a-priori* according to presumed levels of awareness, analogously to previous studies looking at the functional network properties of consciousness (Di Perri et al., 2016; Demertzi et al., 2019). For the main analysis the CAM awake condition was ordered (as a factor in R) before the CAM moderate sedation, which in turn was placed as more aware than the DOC minimally conscious state (MCS) and DOC unresponsive wakefulness syndrome (UWS), respectively. To assess the robustness of our results, we performed a second analysis by substituting the CAM propofol dataset with the LON propofol dataset which comprised an awake and a deep sedation condition (ordered, respectively, Fig. 1F).

3.1. SW dynamic complexity in the brain

Our hypothesis that dynamic SW sample entropy (dSW-E) predicts monotonically decreasing levels of awareness was confirmed using an ordinal logistic regression for both SW measures (Fig. 2: PHI Odds ratios [OR] = 4.14 $p = 0.000006$; C.I. [confidence intervals of odds ratios 2.5%:97.5%] 2.48: 7.77; Sigma OR: 2.48 $p = 0.0002$ C.I. 1.48:4.17). This result was corroborated across different parcellations with different granularities (presented in appendix D). Furthermore, this result was replicated in the second analysis with a different sedation dataset (i.e., LON-DOC datasets = PHI; OR = 2.27 $p = 0.001$ C.I. 1.30:3.93 and Sigma; OR = 2.25 $p = 0.001$, C.I. 1.34:3.74; S2, Fig. 2). This suggests that the unpredictability of dynamic SW architecture reliably scales with increasing levels of awareness.

This consistency is remarkable given that when we calculated the two SW measures (PHI and Sigma) on static graphs (i.e. one graph per participant constructed by averaging across all timepoints (Schroter et al., 2012; Monti et al., 2013)), they were not correlated (Rho = 0.17, $p = 0.2$) and did not yield consistent patterns between conditions and network definitions (see appendix C). Conversely, the two measures of SW when calculated dynamically, proved more informative and showed the same intuitive patterns of decreasing complexity in lower levels of awareness (Fig. 2).

It is important to assess whether these graph theory entropy metrics truly reflect the temporal complexity of the functional architecture (i.e., topology), or can be explained more parsimoniously by lower order metrics such as the dynamic variation in functional connectivity (FC) (van den Heuvel et al., 2017). In fact, the entropy of average positive dynamic FC (chosen as graph theory properties were here calculated on positive correlations (Rubinov and Sporns, 2010; van den Heuvel et al., 2017)) was a significant predictor for levels of awareness across parcellations and datasets (e.g., lower granularity whole brain parcellation for CAM-DOC analysis: OR = 1.63, C.I. = 1.02:2.59, $p = 0.01$, see appendix E for all results). Such results suggest that awareness entails an unpredictability of dynamic global synchronisation levels (measured by brain region timeseries Pearson's correlations). This begs the question whether dynamic SW entropy (dSW-E, Fig. 2) truly reflects the consciousness-predictive complexity of functional topology, or whether SW entropy results may be better explained by the unpredictability of global synchronisation.

To investigate this question, we ran a control ordinal logistic regression analysis that involved the same exact procedure used above (Fig. 1f) with the addition of the sample entropy of dynamic FC (dFC-E) as a covariate predictor. Both SW entropy predictors remained significant in the main analysis (Table 1 and appendix E). However, in the analysis controlling for dFC-E in the LON-DOC dataset, the dSW-E of Sigma for the AAL parcellation lost significance (Table 1), whilst dSW-E results remained significant in all other parcellations despite controlling for dFC-E. Of interest is that PHI showed higher effect sizes than sigma suggesting it to be more sensitive to relevant variation ((Papo et al., 2016), Section 2.5.1, appendix D and F). Of note is also that the complexity of dynamic functional connectivity (dFC-E) tended to display stronger effects when inserted as a covariate with the Sigma measure rather than when inserted with PHI (Table 1).

This control analysis included both dFC-E and dSW-E as co-variate predictors in the same ordinal logistic regression and found the latter remained significant. This suggests that the temporal complexity of SW architecture predicts increasing levels of awareness above and beyond what can be explained by the complexity ("compressibility")

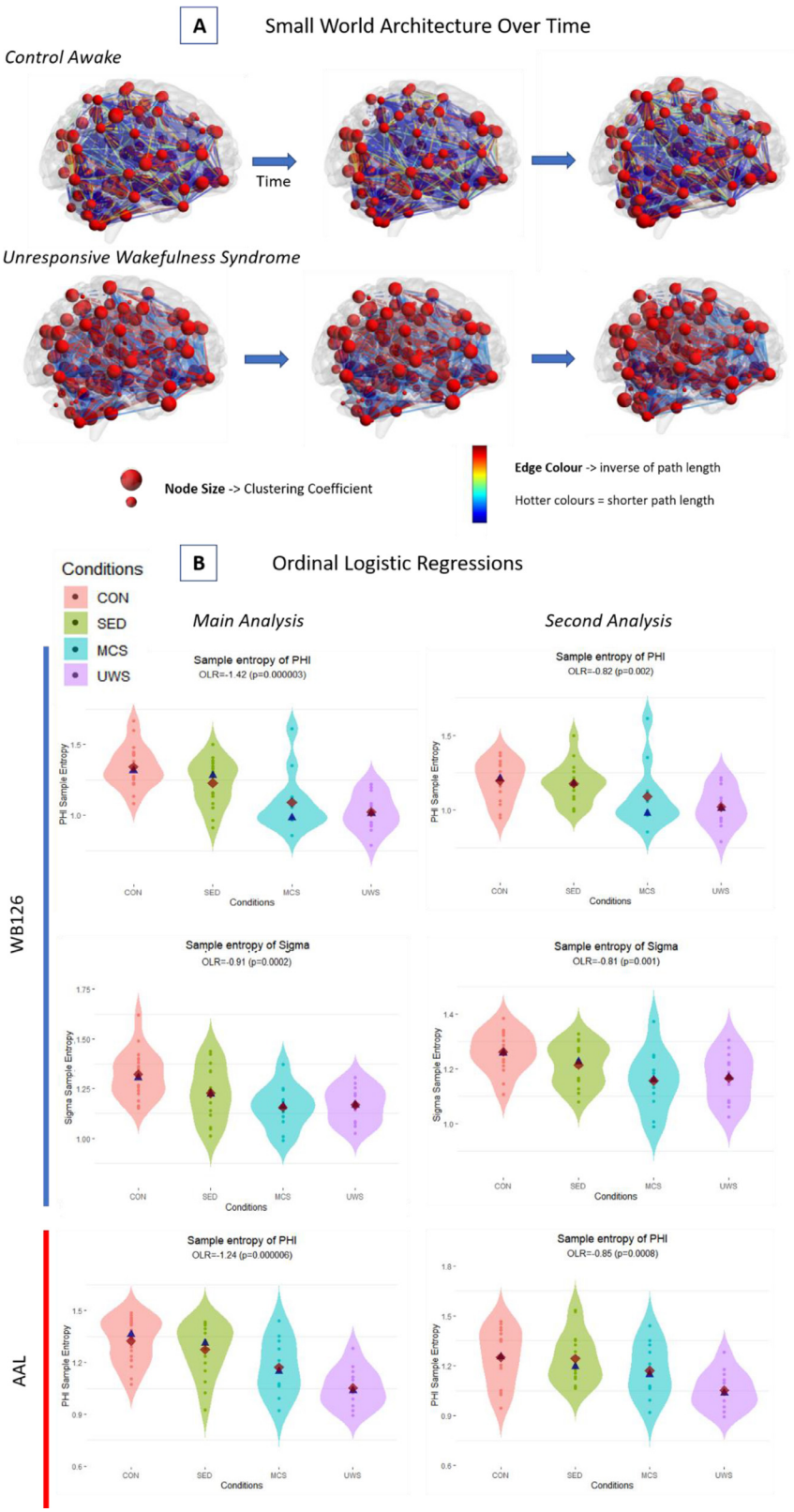

Fig. 2. Dynamic SW properties and ordinal logistic regression results. In the top panel (A) are shown example dynamic SW properties (3 timepoints) overlaid on a brain template (Brainmesh_Ch2withCerebellum; BrainNet viewer Xia et al., 2013). The size of the nodes represents the clustering coefficient of that node, whilst the connections represent the inverse of the path length between the two nodes. The hotter the colour, the shorter the path length (i.e., how easily information can be transmitted between the nodes, not direct connectivity). Shown, for illustrative purposes, (top-left) is an example of a control awake participant (CAM dataset) and an example of an unresponsive wakefulness syndrome patient (DOC dataset; bottom-left). Noticeable is the change in node size (clustering coefficient) and edge colour (path length) over time in the control participant, which is not so prominent in the individual affected by UWS. In the bottom panel (B) violin plots are showing the scaling of dynamic SW sample entropy with levels of awareness for both the main and second analysis. Conditions are ordered (left to right) according to a-priori presumed level of awareness (i.e., Awake > Propofol Sedation > MCS > UWS). The first two rows represent the dynamic PHI and Sigma entropy for a whole brain parcellation with 126 regions (appendix A), respectively. The third row represents dynamic PHI entropy values for the AAL. Blue triangle represents the median, whilst the red diamond represents the mean. OLR = ordinal logistic regression coefficients; UWS = unresponsive wakefulness syndrome; MCS = minimally conscious state; SED = propofol sedation; CON = control awake condition. All ordinal logistic regression values are standardized for comparison.

of dynamic functional connectivity. This may be taken as a strong indication that the dynamic information produced (measured *via* sample entropy (Richman and Moorman, 2000)) by functional topological temporal organisation will decrease with diminishing levels of awareness.

3.2. Dynamic complexity in the brain of the components of small worldness: clustering and path length

To further elucidate these results (Fig. 2), we investigated whether the dSW-E effect could be explained by the complexity of the dynamics

Table 1
Odds ratios and p-values for dSW-E and dFC-E when inserted into the same ordinal logistic regression as covariates. Results for all whole-brain parcellations and the CAM-DOC and LON-DOC analyses.

	Parcellation	SW measure	dSW-E Odds ratios	P-value	dFC-E Odds ratios	P-value
CAM-DOC	WB126	**Φ**	4.52	0.00001	1.15	0.30
Analysis		σ	2.53	0.0002	1.61	0.019
	AAL	**Φ**	3.85	0.00001	0.21	0.22
		σ	2.16	0.00150	1.23	0.070
	WB553	**Φ**	3.22	0.0002	1.09	0.37
LON-DOC	WB126	**Φ**	1.80	0.04	1.42	0.12
Analysis		σ	1.89	0.01	1.55	0.049
	AAL	**Φ**	2.15	0.01	1.12	0.36
		σ	1.32	0.13	1.68	0.021
	WB553	**Φ**	1.92	0.02	1.36	0.16

Table 2
CAM-DOC analysis of different whole brain parcellations. The dynamical complexity of clustering coefficient (dCC-E) and path length (dPL-E), controlled for the dynamical complexity of functional connectivity (dFC-E).

Parcellation	SW component	Clustering Coefficient (CC) and Path Length (PL) dynamic complexity		dFC-E	
		Odds ratio	P-value	Odds ratio	P-value
WB126	dCC-E	4.28	0.000114	0.66	0.119
	dPL-E	3.99	0.000038	0.79	0.211
AAL	dCC-E	10.78	0.000002	0.37	0.003
	dPL-E	5.12	0.000004	0.59	0.045
WB553	dCC-E	4.32	0.003864	0.51	0.093
	dPL-E	3.69	0.000146	0.80	0.247

of the clustering or path length that compose small worldness. We found that both of these components of SW were predictive of levels of awareness despite controlling for the complexity of the underlying FC dynamics (see Table 2). In the CAM-DOC dataset and the lower granularity parcellation the odds ratio was 4.28 (C.I. = 2.06:9.80, p = 0.0001) for the clustering coefficient dynamics (dCC-E) and for the functional connectivity dynamics (dFC-E) the odds ratio was 0.66 (C.I. = 0.31:1.28, p = 0.12). For the path length dynamics (dPL-E), the odds ratio was 3.99 (C.I. = 2.06:8.18, p<0.0001), whilst the odds ratio for dFC-E was 0.79 (C.I. = 0.44:1.41, p = 0.21), when inserted as a covariate in the same model. These results reproduced across different measure implementations (normalised [Muldoon et al., 2016] or non-normalised) and different parcellations (appendix G). Similar results were found for the LON-DOC dataset with the exception of the normalised path length in the lower granularity parcellation and, in the higher granularity parcellation, the clustering coefficient measures and non-normalised path length (see appendix G for full results). This indeed suggests that the dynamics of the integration (path length) and segregation (clustering coefficient) components underlying SW are individually predictive of levels of awareness.

3.3. Dynamic small-world entropy in the cortex, subcortex and cerebellum

Given that dynamic entropy of both SW measures (φ & σ) consistently predicted levels of awareness at the whole-brain level, we sought to explore whether the dSW-E of major cytoarchitectonically distinct subdivisions of the brain (i.e., cortex, subcortex and cerebellum) are relevant to consciousness and differentially explain the above whole-brain effects found in both high and low granularity parcellations.

This analysis is relevant to debates in the literature in which, some postulate the importance of the cortex in consciousness (Tononi et al., 2016; Ledoux and Brown, 2017); whilst others posit an essential role for the subcortex (Carhart-Harris and Friston, 2019; Panksepp, 2011; Solms, 2013).

Given the instability of SW measures when calculated on time-averaged networks, as shown by the inconsistences between previously published results (e.g., 29,31) and in the present study (appendix C), we thought it paramount to assess the convergence of results between different SW implementations (Sigma and PHI). Given the strong convergence of results across control analyses (varying parcellation type, granularity, dataset and SW measures; Table 1; Fig. 2), we continued with one measure. Although Sigma is widely used in the published literature, it is computationally expensive when run on time-varying networks and it is based on a normalisation method that is not completely faithful to the original definition (Watts and Strogatz, 1998). It normalises the network's clustering coefficient to a random network, whilst the original definition states that small world "systems can be highly clustered, like regular lattices, yet have small characteristic path lengths, like random graphs" (Watts and Strogatz, 1998, p.440). The PHI measure on the other hand assesses clustering and path length as divergence from lattice and random networks, respectively (Muldoon et al., 2016, appendix C, 2.5.1). PHI's normalisation method was also specifically designed to be used with weighted networks, thus being more adept at preserving biologically relevant information and controlling for the underlying FC effects (as shown by the difference in dFC-E effects when PHI and Sigma are inserted as covariates in the same analyses; Table 1). Furthermore, PHI seemed to produce higher effect sizes across measures in predicting levels of awareness (Section 3.1, Table 1) and is computationally much more viable. For these reasons we continued analyses with the PHI measures only, having ascertained the convergence of alternative definitions of small-world networks when calculated dynamically.

The complexity of dynamic SW topology had unique predictive power for levels of awareness in the cortical (OR = 3.67 p = 0.000006 C.I. = 2.03:6.62) and subcortical (OR = 6.96 p = 0.000003 C.I. = 3.00:14.88) network definitions. The cerebellar parcellation displays a significant trend (Fig. 3; OR = 1.68, p = 0.02, C.I. = 1.01:2.88; appendix I).

Remarkably, the effect sizes for the subcortex were greater than those of the cortex when inserted in the same ordinal logistic regression as covariates (appendix I), whilst the cerebellum also displayed unique predictive power. The LON-DOC datasets showed convergent results with the exception of the high granularity cortical parcellation (400 nodes; p = 0.08, appendix H). Furthermore, when we added dFC-E as a covariate to dSW-E, both the cortex and subcortex remained significant,

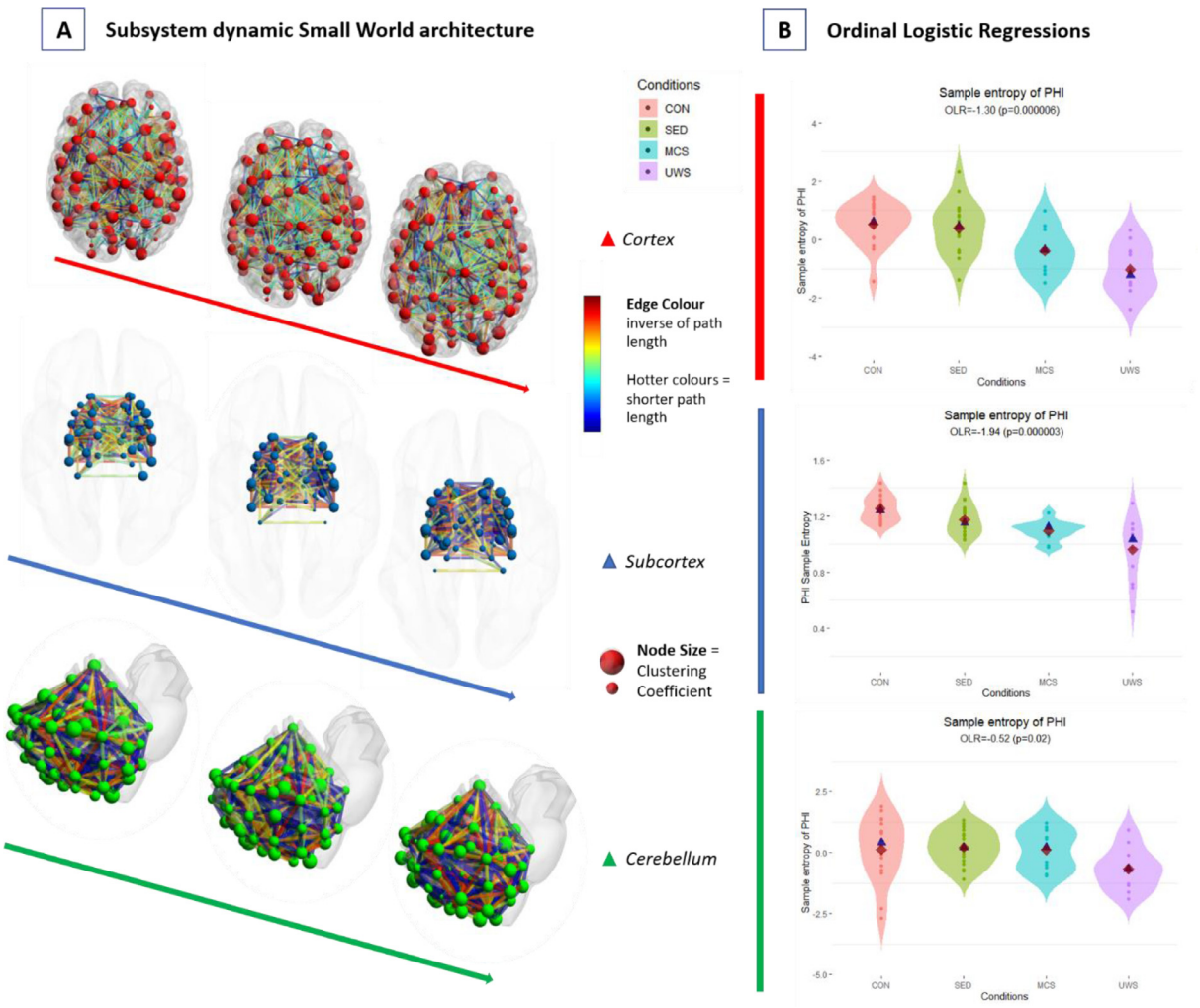

Fig. 3. Subsystem dynamic SW properties and ordinal logistic regression results. In the left panel **(A)** are shown example dynamic SW properties (3 timepoints) for the cortex, subcortex and cerebellum (templates: BrainMesh_Ch2withCerebellum; BrainMesh_ICBM152_smoothed; BrainMesh Cerebellum, respectively, created in BrainNet viewer Xia et al., 2013). Node size represents the clustering coefficient of that node, whilst the connections represent the inverse of the path length between the two nodes. The hotter the colour, the shorter the path length. Shown are three timepoints for the cortex (red nodes; no = 100), subcortex (blue nodes; no = 54) and the cerebellum (green nodes; no = 99), for an awake participant (CAM dataset). In the right panel (B) violin plots are showing the scaling of dynamic PHI sample entropy with levels of awareness. Blue triangle represents the median, whilst the red diamond represents the mean. Conditions are ordered (left to right) according to a-priori presumed levels of awareness (i.e., Awake > Propofol Sedation > MCS > UWS). The first row shows the cortical, the second the subcortical and the last the cerebellar results. OLR = ordinal logistic regression coefficients; UWS = unresponsive wakefulness syndrome; MCS = minimally conscious state; SED = propofol sedation; CON = control awake condition. All ordinal logistic regression values are standardized for comparison.

whilst the cerebellum dSW-E was not significant ($p = 0.055$; Appendix J). When controlling for dFC-E, the sSubcortex dSW-E again had higher odds ratios (OR = 6.23) than the cortex (OR = 3.49) in both datasets, although the cortex violated regression assumptions in the CAM-DOC analysis (Appendix J).

A similar pattern was observed in the LON-DOC dataset (appendix J). These results suggest that the complexity of subcortical dynamic SW topology may be more consistently sensitive to decreasing levels of awareness than the cortex.

We then investigated whether these measures were correlated to behavioural metrics (bedside diagnostic assessments of consciousness-impairment in DOC patients via the Coma Recovery Scale-revised [CRS-r (Giacino et al., 2004)]; and pharmacological plasma propofol concentration metrics (in CAM dataset). This would elucidate the potential relevance of dSW-E to clinically-relevant observable behaviour (in the case of CRS-r) and the amount of propofol found in the blood. We found that subcortex dSW-E was inversely correlated to Propofol plasma concentration in the CAM dataset (rho = −0.38, $p = 0.022$). However, this correlation did not survive Bonferroni correction for the different parcellations and measures used. Propofol plasma concentration is known to correlate with individual differences in consciousness recovery time and the underlying genetic variation relevant to pharmacokinetics (Kansaku et al., 2011). The relationship between subcortical network dynamics and propofol concentration may relate to individual differences in pharmacodynamic effect on the brain and therefore differences in levels of awareness. There was also a correlation between SW entropy of PHI of the cortex and CRS-r (rho = 0.56, $p = 0.004$), but this did not replicate in the higher granularity parcellation. Although this behavioural measure is considered the most comprehensive instrument to detect consciousness at the bedside (Giacino et al., 2004; Edlow et al., 2021) it should be noted that behavioural responsiveness is not a perfect correlate of consciousness (e.g., Owen et al., 2008) and may vary substantially within patients (Wannez et al., 2017). Thus, such a correlation may indicate that cortical dynamic complexity is related to consciousness, but not unequivocally so.

Table 3
Main analyses (CAM-DOC datasets). Predictive power of the complexity of dynamic modularity (dM-E) and participation coefficient (dPC-E) when controlling for functional connectivity complexity (dFC-E). Odds ratios and *p*-values.

Parcellation	dM-E and dPC-E			dFC-E	
	Measure	Odds ratio	P-value	Odds ratio	P-value
Cortex-100	dM-E	1.94	0.00800	1.71	0.02
	dPC-E	1.28	0.17665	1.79	0.02
Subcortex	dM-E	2.61	0.00105	1.60	0.04
	dPC-E	3.06	0.00022	1.80	0.01
Cerebellum	dM-E	2.47	0.00109	1.01	0.48
	dPC-E	3.77	0.00003	1.08	0.39

3.4. Sample entropy of integration and segregation dynamic graph theory metrics for the cortex, subcortex and cerebellum

Given that subcortical dSW-E has more predictive power than the cortex, we sought to investigate whether this striking effect (Fig. 3) is specific to SW or can be generalised to other topological organisation (graph theory) measures that are relevant to consciousness theory. To this end, we chose two measures that are conceptually (in terms of integration and segregation Rubinov and Sporns, 2010; Sporns and Zwi, 2004; Lord et al., 2017) and statistically related to SW (Jarman et al., 2017). The first is modularity, which measures the extent to which a network can be divided, therefore being a proxy measure for segregation in terms of functional differentiation at a network level. The second measure is participation coefficient, that measures to what extend different modules (i.e., functional subdivisions calculated via modularity) of the network are interconnected, therefore indicating the degree of integration in terms of the merging of information from different modules. We analysed these measures as we did SW in the previously described procedure (from Fig. 1D onwards).

Firstly, we established whether the complexity of network dynamics had predictive power in the cortex, subcortex and cerebellum. We found that the complexity of dynamic modularity (dM-E) could predict levels of awareness beyond the complexity of dFC-E in all subsystems (cortex, subcortex and cerebellum see Table 3). The dynamics of participation coefficient had predictive power only in the subcortex and cerebellum (Table 3). In the alternative analysis (with LON-DOC datasets) results did not reproduce for the dM-E of the cortex (see appendix K for full results).

Remarkably, when we inserted the complexity of dynamic participation coefficient (dPC-E) of the different subsystems into the same model, we saw that the odds ratio (OR) of the cerebellum (OR = 2.76; C.I. = 1.46:5.71, $p = 0.001$) was higher than both that of the subcortex (OR = 2.14; C.I. = 1.08:4.44, $p = 0.01$) and cortex (OR = 1.09; C.I. = 0.63:1.90, $p = 0.36$) (appendix M). The complexity of modularity dynamics (dM-E) had higher effect sizes (i.e., odds ratios) in the subcortex (OR = 2.15 C.I. = 1.10:4.42, $p = 0.013$) than the cortex (OR = 1.52; C.I. = 0.86:2.75, $p = 0.07$) and the cerebellum (OR = 1.61; C.I. = 0.86:3.07, $p = 0.06$). These results also reproduced in the second analysis (appendix M).

Using the behavioural scores collected in the original semantic propofol study for the CAM dataset (Adapa et al., 2014) we found that subcortical dPC-E was inversely correlated to reaction time (Rho = −0.40, $p = 0.017$). Speculatively, reaction time may indicate a change in the consciousness-relevant global availability of information (e.g., Global Neuronal Workspace; (Baars, 2005, 2002)). However, we take this correlation as evidence that subcortical dPC-E is relevant to observable behaviour which may only be tangentially related to consciousness proper. Overall, these results suggest that decreasing subcortical complexity of network dynamics (beyond SW) is a characteristic of decreasing levels of awareness.

3.5. Predictive power of dynamic graph theory metrics for between subnetwork dynamics beyond dynamic functional connectivity

Until now we have investigated the predictive power of network dynamics of the whole-brain and of individual subsystems (cortex, subcortex and cerebellum). In Information Integration Theory (Tononi et al., 2016) and other accounts of consciousness (Baars, 2005; Alkire et al., 2008; Lamme, 2006; Shine et al., 2019), the communication between subsystems (e.g., between the cortex and subcortex) has been proposed as fundamental to the emergence of complex awareness. Therefore, we also investigated whether between subsystems network dynamics were predictive of levels of awareness. Specifically, we defined three dynamically varying between-system networks: cortex-cerebellum, cortex-subcortex and subcortex-cerebellum (described in section 2.5). We calculated the dynamic complexity of path length, participation coefficient and modularity. The clustering coefficient and therefore small world propensity could not be calculated as networks defined in this manner are not amenable to this measure (explained in methods, Section 2.5). We found that all between system graphs and network properties displayed dynamics that were predictive of levels of awareness despite controlling for the underlying functional connectivity. Results are presented in Table 4.

3.5.1. Independent predictive power of between and within subsystem network dynamics

We then tested whether between subsystem network dynamics had any independent predictive power compared to within subsystem network dynamics. To this end we inserted all within and between system (cortex, subcortex and cerebellum) dynamic network complexity measures in the same analysis and ran an ordinal logistic regression for each graph theory metric (small worldness, participation coefficient and modularity). We found that for the dynamic complexity of participation coefficient, the cortex (OR = 0.44, C.I. 0.20:0.95, $p = 0.021$), the cerebellum (OR = 2.22, C.I. = 1.01:5.21, $p = 0.027$), the cortex-subcortex network (OR = 2.88, C.I. = 1.21:7.60, $p = 0.01$) and the subcortex-cerebellum (OR = 2.59, C.I. = 0.99:7.07, $p = 0.028$) were significant predictors. For the dynamical complexity of modularity only the subcortex-cerebellar topology was a significant predictor (OR = 2.07, C.I. = 0.97:4.60, $p = 0.03$). Finally, for the dynamical complexity of path length, only the subcortex showed significance (OR = 2.21, C.I. = 1.03:5.00, $p = 0.02$), however the assumptions of the ordinal logistic regression were violated for this model (Brant's test $p < 0.05$).

These results (Table 5) confirm that dynamic network structure between subsystems may also be independently predictive of levels of awareness. Specifically, the dynamic organisation of subcortex in relation to the cortex and cerebellum seems to have independent predictive power compared to other networks. Thus, these analyses support the notion that the mode of communication between cytoarchitectonically differentiated systems of the brain may indeed be important for the emergence of consciousness (Tononi et al., 2016; Di Perri et al., 2016; Alkire et al., 2008; Guldenmund et al., 2013; Spindler et al., 2021).

3.6. Independent predictive power of dynamic graph theory metrics for the cortex, subcortex and cerebellum

Finally, we sought to investigate whether the complexity of the various network properties investigated (small worldness, participation coefficient and modularity) had independent predictive power in the different subsystems (cortex, subcortex and cerebellum). To this end, we inserted all dynamic complexity metrics (dSW-E, dM-E and dPC-E) as covariates in the same ordinal logistic regression as this would permit further interpretation. We found that dSW-E had unique predictive power in the cortex (OR:3.49, C.I. = 1.88:6.89 $p = 0.00007$) and the subcortex (OR:5.12, C.I. = 2.18:13.61 $p = 0.0002$). Conversely, dPC-E had independent predictive power in the cerebellum (OR:3.30, C.I. = 1.73:6.81,

Table 4
Between subsystem ordinal logistic regression results for the dynamic complexity of path length (dPL-E), modularity (dM-E) and participation coefficient (dPC-E).

		Dynamic graph theory complexity		dFC-E	
Network	Measure	Odds ratios	p-value	Odds ratio	p-value
Cortex-cerebellum	dPL-E	4.68	0.00001	0.67	0.10
Cortex-cerebellum	dM-E	2.72	0.00036	1.20	0.23
Cortex-cerebellum	dPC-E	3.50	0.00003	0.96	0.45
Cortex-subcortex	dPL-E	3.72	0.00042	0.76	0.21
Cortex-subcortex	dM-E	1.80	0.01602	1.41	0.10
Cortex-subcortex	dPC-E	4.63	0.00001	0.96	0.45
Subcortex-cerebellum	dPL-E	4.12	0.00046	0.66	0.14
Subcortex-cerebellum	dM-E	2.99	0.00043	1.08	0.39
Subcortex-cerebellum	dPC-E	4.83	0.00001	1.08	0.39

Table 5
Odds ratios and p-values for between and within subsystem network dynamics when inserted into the same ordinal logistic regression. Results for the dynamic complexity of participation coefficient (dPC-E), modularity (dM-E) and path length (dPL-E) presented.

Measure	Cortex		Subcortex		Cerebellum		Cortex-cerebellum		Cortex-subcortex		Subcortex-cerebellum	
	Odds Ratio	p-value	Odds Ratio	p-value	Odds Ratio	p-value	Odds Ratio	p-value	Odds Ratio	p-value	Odds Ratio	p-value
dPC-E	2.20	0.02	1.34	0.20	2.22	0.03	1.01	0.50	2.88	0.01	2.59	0.03
dM-E	1.25	0.23	1.67	0.07	1.23	0.29	1.46	0.17	1.22	0.28	2.07	0.03
dPL-E	1.55	0.13	2.21	0.02	1.00	0.50	2.46	0.07	1.36	0.26	1.04	0.47

Table 6
For main (CAM-DOC) analysis. dM-E, dPC-E and dSW-E inserted in the same ordinal logistic regression as covariates for each subsystem (cortex [two granularities 100 and 400], subcortex, and cerebellum), odds ratios (OR), *p*-values and omnibus brants test presented.

NETS	dPC-E		dM-E		dSW-E	
	Odds ratios	p-value	Odds ratios	*p*-value	Odds ratios	p-value
COR-100	0.79	0.2092	1.71	0.04	3.49	0.00007
COR-400	1.13	0.3228	1.36	0.16	2.28	0.00566
SUB	1.76	0.0749	1.60	0.09	5.12	0.00021
CEREB	3.30	0.0003	1.73	0.06	0.80	0.24885

$p = 0.0003$). See Table 6 for more details for each measure in each subsystem. In the alternative anaesthesia dataset, we found results to not reproduce for the cortex (see appendix N for full analyses). Either way, these results indicate that dSW-E is predictive of levels of awareness in the subcortex when controlling for the dynamics of other network properties, whilst the dynamics of participation coefficient had independent predictive power for the cerebellum. This is a significant result, as theorists have indicated that the cerebellum may not be important for consciousness (Tononi et al., 2016). Our analysis shows that the cerebellum does indeed display uniquely predictive consciousness-relevant dynamics at a network level. Across all subsystems and measures the subcortex had the greatest effect size.

4. Discussion

In consonance with our hypothesis, a key finding of this study is that the temporal complexity of network architecture increases with levels of awareness. We integrate graph theory (Schroter et al., 2012; Monti et al., 2013; Achard et al., 2012; Crone et al., 2014) and dynamics (Luppi et al., 2019; Barttfeld et al., 2015; Huang et al., 2020; Demertzi et al., 2019) to show that the temporal complexity of information architecture reliably scales with levels of awareness. Importantly, we show that the complexities of subcortical changes over time is particularly predictive of levels of awareness. Such cortical and subcortical dynamics possibly underlie the varied streams of contents and states that characterise consciousness as an inherently dynamic phenomenon (Tononi et al., 2016; Carhart-Harris and Friston, 2019; Dehaene and Christen, 2011; James, 1890; Ledoux and Brown, 2017; Panksepp, 2011).

Previously, changes in static (Di Perri et al., 2016; Stamatakis et al., 2010; Naci et al., 2018) and dynamic functional connectivity (Barttfeld et al., 2015; Demertzi et al., 2019; Golkowski et al., 2019; Cavanna et al., 2018) in different states of consciousness have been widely reported. We advance this body of research by showing that the sample entropy of dynamic FC is predictive of levels of awareness; but importantly, we additionally show that network architecture dynamics have consistent explanatory power above and beyond the variations in functional connectivity.

This suggests that awareness has characteristic dynamic global information architectures (topologies) that cannot be reduced to simple FC. In other words, the dynamic re-configuration of the global functional architecture ("the interrelation of parts"), rather than the absolute synchronisation of brain regions, may be particularly important to consciousness. These findings, therefore, speak to theories that posit a global workspace (of information Baars, 2005), or the irreducibility of the whole to its parts (Tononi et al., 2016). In fact, we show that the dynamics of architectures that favour integration and segregation consistently scale with increasing levels of awareness. It is therefore possible that such architectures may contribute to an integrated dynamic global workspace of information across time.

A key result of this study may supply some interpretations in regards to what may be particularly important for consciousness emergence. This is the difference between cortical and subcortical effects. Although the cortex was a significant predictor on its own, we found that the complexity of dynamic subcortical topology is more consistent and powerful in predicting levels of awareness than the cortex. This suggests that the complexity of topological functional dynamics in the subcortex is particularly sensitive to different levels of awareness.

In fact, the subcortical system is thought to provide fundamental (affective, interoceptive and sensory) inputs for cortical processing, and is hypothesised to have underpinned the first subjective experiences in evolutionary history and subsequent phylogenic development of higher-order self-awareness (Carhart-Harris and Friston, 2019; Panksepp, 2011;

Solms, 2013). Despite studies on the dynamics of consciousness tend to focus mainly on the cortex (Barttfeld et al., 2015; Huang et al., 2020; Demertzi et al., 2019), recent evidence (Lutkenhoff et al., 2020a) shows that the complexity of cortical response to perturbation in DOC inversely correlates with atrophy in arousal-related subcortical structures rather than in cortical structures. Of note is that the cortex may have a larger variation between subjects than the subcortex (Salehi et al., 2020; Feilong et al., 2018) which is philogenically older and supports basic physiological functions (Panksepp, 2011). This is especially pertinent in the DOC dataset which is characterised by ischaemic or traumatic damage which may induce a subsequent reorganisation of brain function (e.g., Crone et al., 2014; Lamme, 2006; Lutkenhoff et al., 2020a). Nonetheless, dynamic complexity was calculated using the subject specific timeseries, and therefore did not rely on variability between subjects and conditions (e.g., Huang et al., 2020; Salehi et al., 2020).

Although some authors propose that subcortical structures function as an unconscious modulator of behaviour and cognitive conscious access (Ledoux and Brown, 2017), rather than underpinning basic awareness (Panksepp, 2011; Solms, 2013), these results suggest that investigations into consciousness that focus exclusively on the cortex (Tononi et al., 2016; Baars, 2005), may necessitate further verification in the future (Shewmon et al., 1999). In fact, the present results suggest that investigating subcortical information may aid finer differentiation of different conscious states (Panksepp, 2011; Lutkenhoff et al., 2020a,b) for clinical purposes.

In a similar vein, although some researchers do not consider the cerebellum important for consciousness (Tononi et al., 2016); we found that integration-relevant network dynamics (particularly dPC-E) had predictive power for levels of awareness beyond other network dynamics (dSW-E & dM-E) in this system. Interestingly, theorists have posited that the cerebellum may not be fundamental to consciousness due to its lack of integrative capacity (Tononi et al., 2016). Conversely, our analysis suggests that a network property which is relevant to integration (participation coefficient being a measure of intramodular connectivity) is most predictive in the cerebellum (Table 6). Furthermore, we also show that dPC-E has unique predictive power in the cerebellum even when controlling for the underlying functional connectivity dynamics (Table 3) and the network dynamics of other systems (Section 3.4). These results lend support to notions that the cerebellum may have a discernible role in awareness (Clausi et al., 2017; Johnson et al., 2019).

Furthering our understanding of the network dynamics associated with awareness, we also show that the temporal variation of the network topology between the cortex, subcortex and cerebellum are significant predictors of levels of awareness. Specifically, the dynamic architecture of activity coordination between the subcortex and the cortex and between the subcortex and cerebellum have independent predictive power when participation coefficient is investigated. Beyond suggesting the relevance of systems beyond the cortex to consciousness, this also suggests that typical awareness might be characterised by a dynamic cooperation between the cytoarchitectonically distinct regions (Shine et al., 2019; Spindler et al., 2021).

Another contribution of this paper is the investigation of the relevance of SW as a metric for consciousness. Although several measures of SW have been proposed (Humphries and Gurney, 2008; Muldoon et al., 2016; Telesford et al., 2011); its calculation in static functional brain networks have been problematic (Rubinov and Sporns, 2010). Such issues, other than being evidenced by the inconsistency between previously published studies on consciousness (Schroter et al., 2012; Monti et al., 2013; Luppi et al., 2019; Barttfeld et al., 2015; Achard et al., 2012; Crone et al., 2014), were found within this study (appendix C). Here, conversely, we show that the richness of the dynamics of this topological measure robustly decreases with diminishing levels of awareness, independently of the cause of unconsciousness, dataset, brain region definition, threshold, and different measures of SW. The SW topology implies an information communication architecture that is simultaneously efficient and specialised. We show that the dynamics of these two components underlying SW, path length and clustering coefficient, are individually predictive of levels of awareness. Such SW components are thought to be related to information transmission and cognition in both health and disease (Sporns and Zwi, 2004; van den Heuvel et al., 2008; Bassett and Bullmore, 2017; Tan and Cheong, 2017; Takagi, 2018; Schilling, 2005; Yu et al., 2011; Wu et al., 2012; Achard et al., 2006; Zhu et al., 2020). Therefore, it is possible that the reconfiguration of SW topology over time may indicate variations in information processing (and therefore cognitive states (Bassett and Bullmore, 2017)), which would intuitively increase proportionally to the level of awareness (Carhart-Harris et al., 2014; Tononi et al., 2016; Laureys et al., 2007). In fact, neural variability has been proposed to be essential to normal brain function (Northoff and Huang, 2017; Waschke et al., 2021). Corroborating this point are several lines of research that show how the dynamics of functional networks are related to different types of cognition (e.g., Baars, 2002; Wu et al., 2012; Achard et al., 2006; Zhu et al., 2020). Such cognition-related changes over time would presumably have an overlap with experiential dynamics that are characteristic of awareness.

However, we have also shown that consciousness-relevant topological dynamics are not limited to SW. The sample entropy of dynamic modularity and participation coefficient, may index changes in the formation and inter-communication of dynamic functional subsystems (e.g., in visual attention), and as such may provide a good metric of variations in the stream of conscious contents or cognitive states that is typical for consciousness (Edelman and Gally, 2013; Di Perri et al., 2016; Godwin and Barry, 2015; Huang et al., 2020; Dixon et al., 2017; Margulies et al., 2016). Specifically, we show that, although these measures are predictive beyond functional connectivity dynamics when considered individually, participation coefficient had unique predictive power when in cerebellum. Analogously to SW, participation coefficient and modularity have been shown to be related to cognition and information processing (Godwin and Barry, 2015; Finc et al., 2017; Han et al., 2020; Bertolero et al., 2018; Cohen and Esposito, 2016; Hilger et al., 2017; Arnemann et al., 2015). Thus, these interpretations are complementary to those made above for SW, in that the dynamic entropy of these GTA properties may indicate dynamic variations in information processing state (and therefore, contents of consciousness).

Given the potential existence of many different types (or dimensions) of consciousness, that the dynamic complexity of several graph theory properties may display predictive power, and that these measures display high within condition standard deviations (Figs. 2 & 3); we tentatively suggest that these results may primarily relate to the epi-phenomenology of consciousness. In other words, the dynamic complexity of functional topology necessarily arises with consciousness, but it may not be a sufficient condition for the emergence of awareness.

4.1. Strengths and weaknesses

As for the strengths and weakness of this study; the temporal resolution of the data-collection technique and the sliding window approach constitute a limitation of this study, as it only can measure coarse timescales of brain activity. Furthermore, DOC data is inherently noisy and is characterised by high degrees of variability and misdiagnosis. We selected this subset of participants out of a bigger dataset to ensure the data had acceptable quality. The ordering of conditions into decreasing levels of awareness may be controversial, in that it reduces subjective qualitative states to a two-dimensional quantity, despite being clinically (Laureys et al., 2007; Giacino et al., 2004), theoretically (Carhart-Harris et al., 2014; Tononi et al., 2016), and intuitively justified. Furthermore, there may be potential to confound behavioural responsiveness with awareness in this study. The use of such ordered conditions of awareness as a dependant variable may somewhat mitigate such a problem; however, the behavioural metrics used (coma recovery

scale for DOC and reaction time for moderate anaesthesia) are primarily related to behavioural responsiveness. To date responsiveness is still one of the best markers of conscious awareness as it is routinely used at the bedside (e.g., Ramsay scale for anaesthesia or coma recovery scale for DOC). Behavioural responsiveness, however, is not necessarily equal to awareness (e.g., Crone et al., 2020; Adapa et al., 2014; Giacino et al., 2004; Cohen and Esposito, 2016; Owen et al., 2008; Owen et al., 2008). Nonetheless, the results using behavioural measures support the notion that the approach used herein does have relevance to observable wilful behaviour, which tends to be correlated with consciousness.

Conversely, in light of inconsistencies between previously published studies, the use of different SW measures and related graph theory measures constitute a strength of this study. In fact, the explicit controlling for the dynamic FC (which underlies the graph theory measures) is a first in graph-theory consciousness research and consolidates the robustness and interpretation of results (van den Heuvel et al., 2017). The investigation of between subsystem topology (e.g., cortex to subcortex exclusively, Table 4) is also novel to our knowledge. The additional use of an independent dataset to validate results, and the use of different parcellations (with different brain region definitions but similar numbers (AAL, $N = 116$ and WB126, $N = 126$), and with similar definitions but different granularities (WB125, WB553 described in appendix A), serve to augment assurance in these results (Hallquist and Hillary, 2018).

These control analyses expand on the study by Crone and colleagues (Crone et al., 2020) which investigated the variability over time of graph theory properties, one of which (clustering coefficient) is part of the SW measure. The use of sample entropy also may constitute a development of this study as it takes into account the temporally sequential information inherent in the data in a way that is robust to noise (Varley et al., 2020; Richman and Moorman, 2000; Wang et al., 2014), rather than calculating variability over all available data (see Section 2.6 for further discussion of this measure). Whilst Crone and colleagues focused on dissociating consciousness from responsiveness in a DOC cohort, we adopt a different approach to the same end in showing that the complexity of network dynamics scales across vastly different consciousness-relevant conditions. The present investigation of the independent predictive power of different subsystems in the brain and different graph theory measures also provides an advancement on previous knowledge.

Of interest is that the CAM-DOC analysis tended to produce stronger effect sizes than the LON-DOC analysis (Table 1, Fig. 1, appendices D–N). This may be due to the fact that the anaesthetic condition in the LON dataset was characterised by relatively more sedation than the CAM dataset (Sections 2.1.2 and 2.2.2) and perhaps is less appropriately ordered as in the present study (after control awake condition and before minimally conscious state). Another explanation for the difference in effect sizes between analyses (CAM-DOC and LON-DOC), is that the CAM and DOC datasets were recorded at the same site, using the same scanner, whilst the LON-DOC analysis is effectively a cross-site analysis, potentially introducing confounds in the data. Nonetheless, although the LON dataset did not have sufficient coverage of the cerebellum thus impeding a reproduction of cerebellar specific results, the LON-DOC analysis consistently replicated subcortical results (appendices H–N). This further supports the robustness of subcortical dynamics in predicting different levels of awareness.

5. Conclusion

We conclude, with a reasonable amount of confidence, that the complexity of dynamic topology (in other words: the re-organisation of functional information architecture) does increase with the emerging of awareness. We tentatively suggest that dynamics of information processing architecture reflects changes in cognitive content/mental state which is an intuitive characteristic of the vernacular “stream of consciousness”. The predictive power of the subcortex’s dynamic topology is higher and more consistent compared to that of the cortex or the cerebellum, suggesting that the dynamic re-organisation of this system may be particularly important in typical awareness. The dynamics of functional topology between the subcortex and other systems (cortex and cerebellum) also display unique predictive power. The complexity of dynamic small world architecture is most predictive for the cortex and the subcortex. The participation coefficient, conversely has independent predictive power for the cerebellum.

Data availability

The Coon toolbox is available to download from http://www.nitrc.org/projects/conn. The brain connectivity toolbox, which was used for the graph theory measures can be obtained gratuitously online (https://sites.google.com/site/bctnet/). Sigma was calculated fusing the BCT functions and following the procedure outlined in Humphries et al., 2008. The small world propensity measure code (PHI) can be obtained from https://complexsystemsupenn.com/codedata. The sample entropy function is freely available (https://physionet.org/content/sampen/1.0.0/).

Data to reproduce results and figures is available at: https://github.com/Peter6789/Network_dynamics_data

DOC dataset: Due to patient privacy concerns, data are available upon request by qualified researchers. The UK Health Research Authority mandates that the confidentiality of data is the responsibility of Chief Investigators for the initial studies (in this case, Dr. Allanson and Prof. Menon; and anyone to whom this responsibility is handed – for example, in the context of retirement or transfer to another institution). For researchers interested in working with this dataset, please contact Dr. Judith Allanson (judith.allanson@addenbrookes.nhs.uk), Prof. David Menon (dkm13@cam.ac.uk) and/or Dr. Emmanuel Stamatakis (eas46@cam.ac.uk). Requests will be considered on a case-by-case basis, assessing the feasibility and appropriateness of the proposed study, and the capacity to maintain the required levels of data security, consistent with the original approved Research Ethics approval, and the patient information sheet that was the basis of consent obtained.

CAM dataset: The data are available from the corresponding author upon request.

LON dataset: Freely available from https://openneuro.org/datasets/ds003171/versions/1.0.0

Declaration of Competing Interest

The authors have no competing interests to declare.

Credit authorship contribution statement

Peter Coppola: Conceptualization, Methodology, Software, Validation, Formal analysis, Writing – original draft, Writing – review & editing, Visualization. **Lennart R.B. Spindler:** Software, Formal analysis, Writing – review & editing. **Andrea I. Luppi:** Software, Formal analysis, Writing – review & editing. **Ram Adapa:** Investigation, Resources, Data curation, Writing – review & editing, Funding acquisition. **Lorina Naci:** Conceptualization, Resources, Data curation, Writing – review & editing, Project administration, Funding acquisition. **Judith Allanson:** Conceptualization, Resources, Investigation, Data curation, Writing – review & editing, Project administration. **Paola Finoia:** Investigation, Data curation. **Guy B. Williams:** Investigation, Conceptualization, Writing – review & editing. **John D. Pickard:** Conceptualization, Resources, Writing – review & editing, Project administration, Funding acquisition. **Adrian M. Owen:** Conceptualization, Resources, Writing – review & editing, Project administration, Funding acquisition. **David K. Menon:** Conceptualization, Investigation, Resources, Writing – review & editing, Supervision, Project administration, Funding acquisition. **Emmanuel A. Stamatakis:** Conceptualization, Resources, Methodology, Formal analysis, Investigation, Writing – original draft, Writing – review & editing, Supervision, Project administration, Funding acquisition.

Acknowledgements

This work was supported by grants from the Wellcome Trust Clinical Research Training Fellowship [to RA] (grant number: 083660/Z/07/Z); the UK Medical Research Council (U.1055.01.002.00001.01) [to AMO and JDP]; The James S. McDonnell Foundation [to AMO and JDP]; The Canada Excellence Research Chairs program (215063) [to AMO]; The Canadian Institute for Advanced Research (CIFAR) [to AMO, DKM and EAS]; The National Institute for Health Research (NIHR, UK), Cambridge Biomedical Research Centre and NIHR Senior Investigator Awards [to JDP and DKM]; The British Oxygen Professorship of the Royal College of Anaesthetists [to DKM]; The Evelyn Trust, Cambridge and the East of England Collaboration for Leadership in Applied Health Research and Care fellowship [to JA]; The L'Oreal-Unesco for Women in Science Excellence Research Fellowship [to LN]; The Stephen Erskine Fellowship, Queens' College, University of Cambridge [to EAS]; the Gates Cambridge Trust [to AIL] and the Cambridge Trust [to PC and LRBS]. The research was also supported by the NIHR Brain Injury Healthcare Technology Co-operative based at Cambridge University Hospitals NHS Foundation Trust and University of Cambridge. Computing infrastructure at the Wolfson Brain Imaging Centre (WBIC-HPHI) was funded by the MRC research infrastructure award (MR/M009041/1). We would like to thank Victoria Lupson and the staff in the Wolfson Brain Imaging Centre (WBIC) at Addenbrooke's Hospital for their assistance in scanning. We would also like to thank all the participants for their contribution to this study. Finally, we would also like to thank the reviewers for their very interesting and pertinent comments and suggestions.

Supplementary materials

Supplementary material associated with this article can be found, in the online version, at doi:10.1016/j.neuroimage.2022.119128.

References

Achard, S., Salvador, R., Whitcher, B., Suckling, J., Bullmore, E., 2006. A resilient, low-frequency, small-world human brain functional network with highly connected association cortical hubs. J. Neurosci. 26 (1), 63–72.

Achard, S., Delon-Martin, C., Vertes, P.E., Renard, F., Schenck, M., Schneider, F., et al., 2012. Hubs of brain functional networks are radically reorganized in comatose patients. Proc. Natl. Acad. Sci. 109 (50), 20608–20613.

Adapa, R.M., Davis, M.H., Stamatakis, E.A., Absalom, A.R., Menon, D.K., 2014. Neural correlates of successful semantic processing during propofol sedation. Hum. Brain Mapp. 35 (7), 2935–2949.

Alkire, M.T., Hudetz, A.G., Tononi, G., 2008a. Consciousness and anesthesia. Science 322, 876–880.

Alkire, M.T., Hudetz, A.G., Tononi, G., 2008b. Consciousness and anesthesia NIH Public access. Science 322 (5903), 876–880 (80-).

Arnemann, K.L., Chen, A.J.W., Novakovic-Agopian, T., Gratton, C., Nomura, E.M., D'Esposito, M., 2015. Functional brain network modularity predicts response to cognitive training after brain injury. Neurology 84 (15), 1568–1574.

Baars, B.J., 2002. The conscious access hypothesis. Trends Cogn. Sci. 6 (1), 47–52.

Baars, B.J., 2005. Global workspace theory of consciousness: toward a cognitive neuroscience of human experience. Prog. Brain Res. 150, 45–53.

Barahona, M., Barahona, M., Pecora, L.M., 2002. Synchronization in small-world systems. Phys. Rev. Lett. 89 (5), 054101/1-054101/4.

Barttfeld, P., Uhrig, L., Sitt, J.D., Sigman, M., Jarraya, B., Dehaene, S., 2015. Signature of consciousness in the dynamics of resting-state brain activity. Proc. Natl. Acad. Sci. 112 (3), 887–892 Jan 20.

Bassett, D.S., Bullmore, E.T., 2017. Small-world brain networks revisited. Neuroscientist 23 (5), 499–516.

Bertolero, M.A., Yeo, B.T.T., Bassett, D.S., D'Esposito, M, 2018. A mechanistic model of connector hubs, modularity and cognition. Nat. Hum. Behav. 2 (10), 765–777.

Buzsáki, G., 2007. The structure of consciousness. Nature 446 (7133), 267.

Calhoun, V.D., Wager, T.D., Krishnan, A., Rosch, K.S., Seymour, K.E., Nebel, M.B., et al., 2017. The impact of T1 versus EPI spatial normalization templates for fMRI data analyses. Hum. Brain Mapp. 38 (11), 5331–5342.

Carhart-Harris, R.L., Friston, K.J., 2019. REBUS and the anarchic brain: toward a unified model of the brain action of psychedelics. Pharmacol. Rev. 71 (3), 316–344.

Carhart-Harris, R.L., Leech, R., Hellyer, P.J., Shanahan, M., Feilding, A., Tagliazucchi, E., et al., 2014. The entropic brain: a theory of conscious states informed by neuroimaging research with psychedelic drugs. Front. Hum. Neurosci. 8, 1–22 (1 FEB).

Cavanna, F., Vilas, M.G., Palmucci, M., Tagliazucchi, E, 2018. Dynamic functional connectivity and brain metastability during altered states of consciousness. Neuroimage 180, 383–395. doi:10.1016/j.neuroimage.2017.09.065, [Internet].

Clausi, S., Iacobacci, C., Lupo, M., Olivito, G., Molinari, M., Leggio, M., 2017. The role of the cerebellum in unconscious and conscious processing of emotions: a review. Appl. Sci. 7 (5), 21–24.

Cohen, J.R,.D., Esposito, M., 2016. The segregation and integration of distinct brain networks and their relationship to cognition. J. Neurosci. 36 (48), 12083–12094.

Crone, J.S., Soddu, A., Höller, Y., Vanhaudenhuyse, A., Schurz, M., Bergmann, J., et al., 2014. Altered network properties of the fronto-parietal network and the thalamus in impaired consciousness. NeuroImage Clin. 4, 240–248.

Crone, J.S., Lutkenhoff, E.S., Vespa, P.M., Monti, M.M., 2020. A systematic investigation of the association between network dynamics in the human brain and the state of consciousness. Neurosci. Conscious 2020 (1), 1–14.

Deco, G., Tononi, G., Boly, M., Kringelbach, M.L., 2015. Rethinking segregation and integration: contributions of whole-brain modelling. Nat. Rev. Neurosci. 16 (7), 430–439. doi:10.1038/nrn3963, [Internet]Available from.

Dehaene, S., Christen, Y., 2011. Characterizing consciousness: from cognition to the clinic? Res. Perspect. Neurosci. 18, 55–84.

Delgado-Bonal, A., Marshak, A., 2019. Approximate entropy and sample entropy: a comprehensive tutorial. Entropy 21, 1–37.

Demertzi, A., Tagliazucchi, E., Dehaene, S., Deco, G., Barttfeld, P., Raimondo, F., et al., 2019. Human consciousness is supported by dynamic complex patterns of brain signal coordination. Sci. Adv. 5 (2), 1–11.

Di Perri, C., Bahri, M.A., Amico, E., Thibaut, A., Heine, L., Antonopoulos, G., et al., 2016. Neural correlates of consciousness in patients who have emerged from a minimally conscious state: a cross-sectional multimodal imaging study. Lancet Neurol. 15 (8), 830–842. doi:10.1016/S1474-4422(16)00111-3, [Internet]Available from:.

Dixon, M.L., Andrews-Hanna, J.R., Spreng, R.N., Irving, Z.C., Mills, C., Girn, M., et al., 2017. Interactions between the default network and dorsal attention network vary across default subsystems, time, and cognitive states. Neuroimage 147, 632–649 (December 2016).

Edelman, G.M., Gally, J.A., 2013. Reentry: a key mechanism for integration of brain function. Front. Integr. Neurosci. 7, 1–6 (August).

Edlow, B.L., Claassen, J., Schiff, N.D., Greer, D.M., 2021. Recovery from disorders of consciousness: mechanisms, prognosis and emerging therapies. Nat. Rev. Neurol. 17 (3), 135–156. doi:10.1038/s41582-020-00428-x, [Internet]Available from.

Feilong, M., Nastase, S.A., Guntupalli, J.S., Haxby, J.V, 2018. Reliable individual differences in fine-grained cortical functional architecture. Neuroimage 183, 375–386. doi:10.1016/j.neuroimage.2018.08.029, [Internet](August)Available from.

Shewmon, D.A., Holmes, G.L., Byrne, P.A., 1999. Consciousness in congenitally decorticate children: developmental vegetative state as self-fulfilling prophecy. Dev. Med. Child Neurol. 41 (6), 364–374.

Finc, K., Bonna, K., Lewandowska, M., Wolak, T., Nikadon, J., Dreszer, J., et al., 2017. Transition of the functional brain network related to increasing cognitive demands. Hum. Brain Mapp. 38 (7), 3659–3674.

Giacino, J.T., Kalmar, K., Whyte, J., 2004. The JFK coma recovery scale-revised: measurement characteristics and diagnostic utility11No commercial party having a direct financial interest in the results of the research supporting this article has or will confer a benefit upon the authors or upon an. Arch. Phys. Med. Rehabil. 85 (12), 2020–2029.

Godwin, D., Barry, R.L., Marois, R., 2015a. Breakdown of the brain's functional network modularity with awareness. Proc. Natl. Acad. Sci. (36), 201414466.

Godwin, D., Barry, R.L., Marois, R., 2015b. Breakdown of the brain's functional network modularity with awareness. Proc. Natl. Acad. Sci., 201414466.

Golkowski, D., Larroque, S.K., Vanhaudenhuyse, A., Plenevaux, A., Boly, M., Di Perri, C., et al., 2019. Changes in whole brain dynamics and connectivity patterns during sevoflurane- a nd propofol-induced unconsciousness identified by functional magnetic resonance imaging. Anesthesiology 130 (6), 898–911.

Guldenmund, P., Demertzi, A., Boveroux, P., Boly, M., Vanhaudenhuyse, A., Bruno, M.-.A., et al., 2013. Thalamus, brainstem and salience network connectivity changes during propofol-induced sedation and unconsciousness. Brain Connect. 3 (3), 273–285 Apr 3.

Hallquist, M.N., Hillary, F.G., 2018. Graph theory approaches to functional network organization in brain disorders: a critique for a brave new small-world. Netw. Neurosci. 3 (1), 1–26 Apr 12.

Han, K., Chapman, S.B., Krawczyk, D.C., 2020. Cognitive Training reorganizes network modularity in traumatic brain injury. Neurorehabil. Neural Repair 34 (1), 26–38.

Hilger, K., Ekman, M., Fiebach, C.J., Basten, U., 2017. Intelligence is associated with the modular structure of intrinsic brain networks. Sci. Rep. 7 (1), 1–12. doi:10.1038/s41598-017-15795-7, [Internet]Available from.

Huang, Z., Zhang, J., Wu, J., Mashour, G.A., Hudetz, A.G., 2020. Temporal circuit of macroscale dynamic brain activity supports human consciousness. Sci. Adv. 6 (11), 1–15.

Humphries, M.D., Gurney, K., 2008a. Network "small-world-ness": a quantitative method for determining canonical network equivalence. PLoS One 3 (4) Apr 30.

Humphries, M.D., Gurney, K., 2008b. Network "small-world-ness": a quantitative method for determining canonical network equivalence. PLoS One 3 (4).

James, W., 1890. The Principles Of Psychology. Pantianos Classics.

Jarman, N., Steur, E., Trengove, C., Tyukin, I.Y., Van Leeuwen, C., 2017. Self-organisation of small-world networks by adaptive rewiring in response to graph diffusion. Sci. Rep. 7 (1), 1–9. doi:10.1038/s41598-017-12589-9, [Internet]Available from.

Johnson, J.F., Belyk, M., Schwartze, M., Pinheiro, A.P., Kotz, S.A., 2019. The role of the cerebellum in adaptation: ALE meta-analyses on sensory feedback error. Hum. Brain Mapp. 40 (13), 3966–3981.

Kansaku, F., Kumai, T., Sasaki, K., Yokozuka, M., Shimizu, M., Tateda, T., et al., 2011. Individual differences in pharmacokinetics and pharmacodynamics of anesthetic agent

propofol with regard to CYP2B6 and UGT1A9 genotype and patient age. Drug Metab. Pharmacokinet. 26 (5), 532–537.
Kolmogorov, 1965. Three approaches to the quantitative definition of information. Probl. Peredachi Inform. 1 (1), 3–11.
Lake, D.E., Richman, J.S., Griffin, M.P., Moorman, R., 2002. Sample entropy analysis of neonatal heart rate variability. Am J Physiol Regul Integr Comp Physiol 283, R789–R797.
Lamme, V.A.F., 2006. Towards a true neural stance on consciousness. Trends Cogn. Sci. 10 (11), 494–501.
Laureys, S., Perrin, F., Brédart, S., 2007. Self-consciousness in non-communicative patients. Conscious Cogn. 16 (3), 722–741.
Ledoux, J.E., Brown, R., 2017. A higher-order theory of emotional consciousness. Proc. Natl. Acad. Sci. USA 114 (10), E2016–E2025.
Lord, L.D., Stevner, A.B., Deco, G., Kringelbach, M.L., 2017. Understanding principles of integration and segregation using whole-brain computational connectomics: implications for neuropsychiatric disorders. Philos. Trans. R. Soc. A 375, 1–21 Royal Society.
Luppi, A.I., Stamatakis, E.A., 2020. Combining network topology and information theory to construct representative brain networks. Netw. Neurosci. 1–29.
Luppi, A.I., Craig, M.M., Pappas, I., Finoia, P., Williams, G.B., Allanson, J., et al., 2019. Consciousness-specific dynamic interactions of brain integration and functional diversity. Nat. Commun. 10 (1), 1–12.
Lutkenhoff, E.S., Johnson, M.A., Casarotto, S., Massimini, M., Monti, M.M., 2020a. Subcortical atrophy correlates with the perturbational complexity index in patients with disorders of consciousness. Brain Stimul. 13 (5), 1426–1435. doi:10.1016/j.brs.2020.07.012, [Internet]Available from.
Lutkenhoff, E.S., Wright, M.J., Shrestha, V., Real, C., McArthur, D.L., Buitrago-Blanco, M., et al., 2020b. The subcortical basis of outcome and cognitive impairment in TBI: a longitudinal cohort study. Neurology 95, 2398–2408 p..
Mitchell, M., 2011. Complexity: A Guided Tour, (1st ed.) Oxford University Press.
Monti, M.M., Lutkenhoff, E.S., Rubinov, M., Boveroux, P., Vanhaudenhuyse, A., Gosseries, O., et al., 2013a. Dynamic change of global and local information processing in propofol-induced loss and recovery of consciousness. PLoS Comput. Biol. 9 (10).
Monti, M.M., Lutkenhoff, E.S., Rubinov, M., Boveroux, P., Vanhaudenhuyse, A., Gosseries, O., et al., 2013b. Dynamic change of global and local information processing in propofol-induced loss and recovery of consciousness. PLoS Comput. Biol. 9 (10).
Muldoon, S.F., Bridgeford, E.W., Bassett, D.S., 2016. Small-world propensity and weighted brain networks. Sci. Rep. 6, 1–13. doi:10.1038/srep22057, [Internet](February)Available from.
Naci, L., Haugg, A., MacDonald, A., Anello, M., Houldin, E., Naqshbandi, S., et al., 2018. Functional diversity of brain networks supports consciousness and verbal intelligence. Sci. Rep. 8 (1), 1–15. doi:10.1038/s41598-018-31525-z, [Internet].
Northoff, G., Huang, Z., 2017. How do the brain's time and space mediate consciousness and its different dimensions? Temporo-spatial theory of consciousness (TTC). Neurosci. Biobehav. Rev. 80 (May), 630–645.
Omidvarnia, A., Zalesky, A., Mansour, L.S., Van De Ville, D., Jackson, G.D., Pedersen, M, 2021. Temporal complexity of fMRI is reproducible and correlates with higher order cognition. Neuroimage 230, 117760. doi:10.1016/j.neuroimage.2021.117760.
Owen, A.M., Coleman, M.R., Boly, M., Davis, M.H., Laureys, S., Pickard, J.D., 2008. Detecting awareness in the vegetative state. Ann. N.Y. Acad. Sci. 1129, 130–138 (September).
Panksepp, J., 2011. The basic emotional circuits of mammalian brains: do animals have affective lives? Neurosci. Biobehav. Rev. 35 (9), 1791–1804. doi:10.1016/j.neubiorev.2011.08.003, [Internet]Available from.
Papo, D., Zanin, M., Martínez, J.H., Buldú, J.M., 2016. Beware of the small-world neuroscientist!. Front. Hum. Neurosci. 10. doi:10.3389/fnhum.2016.00096/abstract, [Internet]Mar 8Available from:.
Parkes, L., Fulcher, B., Yücel, M., Fornito, A., 2018. An evaluation of the efficacy, reliability, and sensitivity of motion correction strategies for resting-state functional MRI. Neuroimage 171, 415–436. doi:10.1016/j.neuroimage.2017.12.073, [Internet](July 2017).
Pedersen, M., Omidvarnia, A., Walz, J.M., Zalesky, A., Jackson, G.D., 2017. Spontaneous brain network activity: analysis of its temporal complexity. Netw. Neurosci. 1 (2), 100–115.
Power, J.D., Plitt, M., Gotts, S.J., Kundu, P., Voon, V., Bandettini, P.A., et al., 2018. Ridding fMRI data of motion-related influences: removal of signals with distinct spatial and physical bases in multiecho data. Proc. Natl. Acad. Sci. USA 115 (9), E2105–E2114.
Preti, M.G., Bolton, T.A., Van De Ville, D., 2017. The dynamic functional connectome: state-of-the-art and perspectives. Neuroimage 160, 41–54 (December 2016).
Richman, J.S., Moorman, J.R., 2000. Physiological time-series analysis using approximate entropy and sample entropy Physiological time-series analysis using approximate entropy and sample entropy. Cardiovasc. Res. 2039–2049.
Rubinov, M., Sporns, O., 2010. Complex network measures of brain connectivity: uses and interpretations. Neuroimage 52 (3), 1059–1069. [Internet]SepAvailable from: http://www.ncbi.nlm.nih.gov/pubmed/19819337.
Rubinov, M., Sporns, O., 2011. Weight-conserving characterization of complex functional brain networks. Neuroimage 56 (4), 2068–2079. doi:10.1016/j.neuroimage.2011.03.069, [Internet]Available from.
Salehi, M., Greene, A.S., Karbasi, A., Shen, X., Scheinost, D., Constable, R.T., 2020. There is no single functional atlas even for a single individual: functional parcel definitions change with task. Neuroimage 208, 116366. doi:10.1016/j.neuroimage.2019.116366, [Internet](November 2019)Available from.
Schilling, M.A., 2005. A "small-world" network model of cognitive insight. Creat. Res. J. 17, 131–154 p..
Schroter, M.S., Spoormaker, V.I., Schorer, A., Wohlschlager, A., Czisch, M., Kochs, E.F., et al., 2012. Spatiotemporal reconfiguration of large-scale brain functional networks during propofol-induced loss of consciousness. J. Neurosci. 32 (37), 12832–12840.
Shine, J.M., Breakspear, M., Bell, P.T., Ehgoetz Martens, K., Shine, R., Koyejo, O., et al., 2019. Human cognition involves the dynamic integration of neural activity and neuromodulatory systems. Nat. Neurosci. 22 (2), 289–296. doi:10.1038/s41593-018-0312-0, [Internet]Available from.
Solms, M., 2013. The conscious Id. Neuropsychoanalysis 15 (1), 5–19.
Spindler, L.R.B., Luppi, A.I., Adapa, R.M., Craig, M.M., Coppola, P., Peattie, A.R.D., et al., 2021. Dopaminergic brainstem disconnection is common to pharmacological and pathological consciousness perturbation. Proc. Natl. Acad. Sci. USA 118 (30), 1–11.
Sporns, O., Zwi, J.D., 2004. The small world of the cerebral cortex. Neuroinformatics 2, 145–162.
Stamatakis, E.A., Adapa, R.M., Absalom, A.R., Menon, D.K., 2010. Changes in resting neural connectivity during propofol sedation. PLoS One 5 (12), 1–11.
Takagi, K., 2018. Information-based principle induces small-world topology and self-organized criticality in a large scale brain network. Front. Comput. Neurosci. 12, 1–10 (August).
Takagi, K., 2020. Principles of mutual information maximization and energy minimization affect the activation patterns of large scale networks in the brain. Front. Comput. Neurosci. 13, 1–16 (January).
Tan, T.L., Cheong, S.A., 2017. Statistical complexity is maximized in a small-world brain. PLoS One 12 (8), 1–15.
Tan, X., Zhou, Z., Gao, J., Meng, F., Yu, Y., Zhang, J., et al., 2019. Structural connectome alterations in patients with disorders of consciousness revealed by 7-tesla magnetic resonance imaging. NeuroImage Clin. 22, 101702. doi:10.1016/j.nicl.2019.101702, [Internet](September 2018)Available from.
Telesford, Q.K., Joyce, K.E., Hayasaka, S., Burdette, J.H., Laurienti, P.J., 2011. The ubiquity of small-world networks. Brain Connect. 1 (5), 367–375.
Tononi, G., Edelman, G.M., 1998. Consciousness and complexity. Science 282 (5395), 1846–1851 (80-).
Tononi, G., Boly, M., Massimini, M., Koch, C., 2016. Integrated information theory: from consciousness to its physical substrate. Nat. Rev. Neurosci. 17 (7), 450–461.
van den Heuvel, M.P., Stam, C.J., Boersma, M., 2008. Hulshoff Pol HE. Small-world and scale-free organization of voxel-based resting-state functional connectivity in the human brain. Neuroimage 43 (3), 528–539. doi:10.1016/j.neuroimage.2008.08.010, [Internet]Available from:.
van den Heuvel, M.P., de Lange, S.C., Zalesky, A., Seguin, C., Yeo, B.T.T., Schmidt, R., 2017. Proportional thresholding in resting-state fMRI functional connectivity networks and consequences for patient-control connectome studies: issues and recommendations. Neuroimage 152, 437–449. doi:10.1016/j.neuroimage.2017.02.005, [Internet](February).
Varley, T.F., Luppi, A.I., Pappas, I., Naci, L., Adapa, R., Owen, A.M., et al., 2020. Consciousness & brain functional complexity in propofol anaesthesia. Sci Rep. 10 (1), 1–13.
Wang, Z., Li, Y., Childress, A.R., Detre, J.A., 2014. Brain entropy mapping using fMRI. PLoS One 9 (3), 1–8.
Wannez, S., Heine, L., Thonnard, M., Gosseries, O., Laureys, S., 2017. The repetition of behavioral assessments in diagnosis of disorders of consciousness. Ann. Neurol. 81 (6), 883–889.
Waschke, L., Kloosterman, N.A., Obleser, J., Garrett, D.D., 2021. Behavior needs neural variability. Neuron 109 (5), 751–766. doi:10.1016/j.neuron.2021.01.023, [Internet]Available from.
Watts, D., Strogatz, S., 1998. Collective dynamics of networks. Nature 393 (6684), 440–442.
Weiler, M., Casseb, R.F., de Campos, B.M., Crone, J.S., Lutkenhoff, E.S., Vespa, P.M., Monti, M.M., 2021. Evaluating denoising strategies in resting-state fMRI in traumatic brain injury (EpiBioS4Rx). Biorxiv. https://doi.org/10.1101/2021.12.10.472139.
Weng, L., Xie, Q., Zhao, L., Zhang, R., Ma, Q., Wang, J., et al., 2017. Abnormal structural connectivity between the basal ganglia, thalamus, and frontal cortex in patients with disorders of consciousness. Cortex 90, 71–87. doi:10.1016/j.cortex.2017.02.011, [Internet]Available from.
Wu, J., Zhang, J., Liu, C., Liu, D., Ding, X., Zhou, C., 2012. Graph theoretical analysis of EEG functional connectivity during music perception. Brain Res. 1483, 71–81. doi:10.1016/j.brainres.2012.09.014, [Internet]Available from.
Xia, M., Wang, J., He, Y., 2013. Brainnet viewer: a network visualization tool for human brain connectomics. PLoS One 8 (7), 1–15.
Yao, Z., Hu, B., Xie, Y., Moore, P., Zheng, J., 2015. A review of structural and functional brain networks: small world and atlas. Brain Inform. 2 (1), 45–52.
Yu, Q., Sui, J., Rachakonda, S., He, H., Pearlson, G., Calhoun, V.D., 2011. Altered small–world brain networks in temporal lobe in patients with schizophrenia performing an auditory oddball task. Front. Syst. Neurosci. 5, 1–13 (FEBRUARY 2011).
Zhang, S., Rogers, B.P., Morgan, V.L., Chang, C., 2020. Association between fMRI brain entropy features and behavioral measures. In: Proceedings of the SPIE, p. 30.
Zhu, Y., Lu, T., Xie, C., Wang, Q., Wang, Y., Cao, X., et al., 2020. Functional disorganization of small-world brain networks in patients with ischemic leukoaraiosis. Front. Aging Neurosci. 12, 1–12 (July).
Margulies, D.S., Ghosh, S.S., Goulas, A., Falkiewicz, M., Huntenburg, J.M., Langs, G., et al., 2016. Situating the default-mode network along a principal gradient of macroscale cortical organization. Proc. Natl. Acad. Sci. USA 113 (44), 12574–12579. [Internet]Available from http://www.ncbi.nlm.nih.gov/pubmed/27791099.